Acta Biomaterialia xxx (xxxx) xxx

Contents lists available at ScienceDirect

Acta Biomaterialia

journal homepage: www.elsevier.com/locate/actbio

Full length article

A comprehensive experimental analysis of the local passive response across the healthy porcine left ventricle

Nicolás Laita[a,*], Alejandro Aparici-Gil[a,b], Aida Oliván-Viguera[a,b,c], Alba Pérez-Martínez[a,b,c], Miguel Ángel Martínez[a,b], Manuel Doblaré[a,b,c,d], Estefanía Peña[a,b]

[a] Aragon Institute of Engineering Research (I3A), University of Zaragoza-Spain Spain
[b] Biomedical Research Networking Center in Bioengineering, Biomaterials and Nanomedicine (CIBER-BBN)-Spain Spain
[c] Aragon Institute of Health Research (IIS Aragon)-Spain Spain
[d] Nanjing Tech University-China China

ARTICLE INFO

Article history:
Received 29 April 2024
Revised 7 August 2024
Accepted 20 August 2024
Available online xxx

Keywords:
Porcine cardiac tissue
Experimental characterization
In vitro testing
True biaxial
Simple triaxial shear
Confined compression
Age impact
Local mechanical behavior differences

ABSTRACT

This work provides a comprehensive characterization of porcine myocardial tissue, combining true biaxial (TBx), simple triaxial shear (STS) and confined compression (CC) tests to analyze its elastic behavior under cyclic loads. We expanded this study to different zones of the ventricular free wall, providing insights into the local behavior along the longitudinal and radial coordinates. The aging impact was also assessed by comparing two age groups (4 and 8 months). Resulting data showed that the myocardium exhibits a highly nonlinear hyperelastic and incompressible behavior. We observed an anisotropy ratio of 2-2.4 between averaged peak stresses in TBx tests and 1-0.59-0.40 orthotropy ratios for normalised fiber-sheet-normal peak stresses in STS tests. We obtained a highly incompressible response, reaching volumetric pressures of 2-7 MPa for perfused tissue in CC tests, with notable differences when fluid drainage was allowed, suggesting a high permeability. Regional analysis showed reduced stiffness and anisotropy (20-25%) at the apical region compared to the medial, which we attributed to differences in the fiber field dispersion. Compressibility also increased towards the epicardium and apical regions. Regarding age-related variations, 8-month animals showed stiffer response (at least 25% increase), particularly in directions where the mechanical stress is absorbed by collagenous fibers (more than 90%), as supported by a histological analysis. Although compressibility of perfused tissue remained unchanged, permeability significantly reduced in 8-month-old animals. Our findings offer new insights into myocardial properties, emphasizing on local variations, which can help to get a more realistic understanding of cardiac mechanics in this common animal model.

Statement of significance

In this work, we conducted a comprehensive analysis of the passive mechanical behavior of porcine myocardial tissue through biaxial, triaxial shear, and confined compression tests. Unlike previous research, we investigated the variation in mechanical response across the left ventricular free wall, conventionally assumed homogeneous, revealing differences in terms of stiffness and compressibility. Additionally, we evaluated age-related effects on mechanical properties by comparing two age groups, observing significant variations in stiffness and permeability. To date, there has been no such in-depth exploration of myocardial elastic response and compressibility considering regional variations along the wall and may contribute to a better understanding of the cardiac tissue's passive mechanical response.

* Corresponding author.
E-mail address: nlaita@unizar.es (N. Laita).

https://doi.org/10.1016/j.actbio.2024.08.028
1742-7061/

Please cite this article as: N. Laita, A. Aparici-Gil, A. Oliván-Viguera et al., A comprehensive experimental analysis of the local passive response across the healthy porcine left ventricle, Acta Biomaterialia, https://doi.org/10.1016/j.actbio.2024.08.028

1. Introduction

Cardiac mechanics is usually delineated into active and passive response, with passive mechanics, especially that related to the left ventricle (LV), being determinant for the overall cardiac function [1,2]. Besides, it also has a significant influence on various cardiac pathologies, including diastolic heart failure [3,4] and myocardial infarction (MI) [5,6]. Focusing on MI, it has been shown that the mechanical properties of the infarcted myocardium are closely related to the preceding physiological ones [5,6]. Research by Fomovsky et al. indicated high variability in post-MI properties based on the selected animal model [6] and the infarction location [7]. Their study concluded that local deformations at the infarction site strongly influence its subsequent structure and properties, highlighting the need to analyze, not only the overall mechanical behavior of the myocardium, but the local variations throughout the entire ventricle. Moreover, tissue-engineered cardiac grafts have emerged as a promising therapeutic strategy post-MI [8–10], being the differentiation of stem cells to cardiomyocytes heavily influenced by their mechanical environment [11–14]. Hence, there is a pressure to replicate the mechanical characteristics of the original tissue to facilitate the best coupling between the native and the newly-developed tissue [14,15]. Therefore, a thorough comprehension of the passive mechanical properties of myocardial tissue is imperative to advance towards efficient models and enhanced therapeutic approaches.

Diverse experimental studies have been conducted to elucidate the elastic mechanical response of cardiac tissue. A prevalent approach is *in vitro* testing of biopsied cardiac tissue samples in pure deformation modes. Apart from early uniaxial studies [16], planar equibiaxial extension tests (EBx) were performed on parallel-to-the-epicardium sheets of myocardial tissue of the left ventricular free wall (LVFW) of canine hearts [17,18]. Later, EBx characterization was extended to true biaxial characterization (TBx) to assess the direction-dependent and cross-coupling effects in canine [19,20], ovine [21,22] and murine [23] LV and RV myocardium. The derived results suggested a transversely isotropic response for the cardiac tissue. However, as LeGrice demonstrated [24], the myocardium exhibits a well-structured three-dimensional distribution, with three mechanical principal constitutive directions: the muscle fibers (f), the sheet in-plane direction (s), and the normal to the cleavage planes (n). This FSN configuration implies a local orthotropic behavior, suggesting that biaxial testing alone is insufficient for a complete three-dimensional characterization [25]. Besides, the relative sliding of myocardial layers plays a crucial role during several stages of cardiac cycle [24,26]. Thus, simple triaxial shear tests (STS) were introduced in porcine hearts [27] and later in human hearts, combined with TBx tests [28], confirming the orthotropic response of myocardial tissue. Recent studies characterised the mechanical response variation among the LVFW, RVFW, and intraventricular septum (IVS) in porcine [29] and murine [30] hearts through TBx tests, as well as in ovine hearts through tensile and shear testing [31]. Ahmad et al. aimed to assess the response at different stages of organ development in porcine hearts [32]. More recently, a novel numerical-experimental approach, focused on the optimality of a complete 3D characterization, was proposed by Avazmohammadi and colleagues, combining STS and pure shear tests (PTS) in ovine cardiac tissue [33].

Despite this extensive elastic characterization of myocardium, it is normally described in averaged terms, without emphasizing on the important local variations that do exist within the tissue. As stated, there are some studies which did attempt to account for local heterogeneities between tissue from RVFW, LVFW and IVS [20,22,28–31]. However, the variation in mechanical response within the LV cavity has been limitedly explored. Specifically, Demer et al. [17] reported differences between the apical and medial LVFW, albeit providing only a qualitative comparison. Ghaemi et al. [22] tested medial and apical samples without observing significant differences, as did not Sommer et al. [28] between the basal and medial zones. The variation along the radial axis (from endocardium to epicardium) has also been explored, with no obvious differences recorded [20,28,34]. Notably, a clear distinct behavior between epicardial and endocardial membranes versus the myocardium has been demonstrated [35,36]. Therefore, while existing results suggest a homogeneous behavior across the LVFW, these studies have been limited to a qualitative evaluation of the local response. None of them has undertaken a more comprehensive characterization of the mechanical response throughout the LVFW.

In addition to these complex elastic properties, tissue compressibility, often overlooked in computational studies, has gained attention in recent research [37–39]. Traditionally, the myocardium is assumed to be incompressible due to its high fluid content [25,33,40,41]. However, it is widely accepted that the myocardium exhibits a 'dynamic' *in vivo* volumetric variations of up to 20% occurring throughout the cardiac cycle [42–48]. This phenomenon is normally attributed to the coronary blood flow, known to vary in volume by 20-40% during the cycle [49,50]. Furthermore, the study by Avazmohammadi et al. demonstrated that this compressibility is not spatially homogeneous, showing heterogeneities along both radial and longitudinal directions [48]. The recent study conducted by Liu et al. [39] highlighted the significance of incorporating compressive behavior in computational models, reaching up to 40% differences in peak stress values along the cardiac wall, as well as a superior fit of wall thickness variation over the cardiac cycle. While this 'dynamic' compressibility has been well explored, questions regarding its ability to fully explain myocardium volumetric variation *in vivo* remain to be answered [42]. In contrast, the intrinsic compressibility of myocardial tissue has not been as extensively analyzed. McEvoy et al. [37] is the only study attempting to quantify it, and only for the myocardium as a whole. Notably, the experimental quantification of the extensive and shear response and the compressive properties has been traditionally treated independently, and, to the best of our knowledge, no attempt has been made to integrate both studies under the same testing methodology.

In this study, we conducted a comprehensive experimental characterization of the passive response of porcine cardiac tissue using TBx and STS tests, complemented by an evaluation of tissue compressibility through confined compression tests (Fig. 1). To thoroughly examine local variations in mechanical properties, we selected samples from distinct positions within the LVFW, with specific attention to differences between the antero-apical and antero-medial areas, which are associated with two prevalent infarction models (left descendant and left circumflex coronary artery infarction models, respectively). Additionally, we considered animals of two different ages to investigate how the mechanical response evolves over time. To our knowledge, this research represents the first attempt to integrate the study all mechanical tests and constitutive properties *in vitro* for the same animal model and under identical test conditions. Moreover, our study provides an exhaustive analysis of the variation in the mechanical response along the LVFW, which is normally explored globally. This expanded characterization of local heterogeneities across the LV volume holds particular significance to analyze the impact of diverse infarct models, given the substantial influence of the position on the mechanical properties of the infarcted tissue. We hope that our findings will contribute to a deeper understanding of the ventricular passive response, ultimately facilitating more precise descriptions of the myocardial tissue.

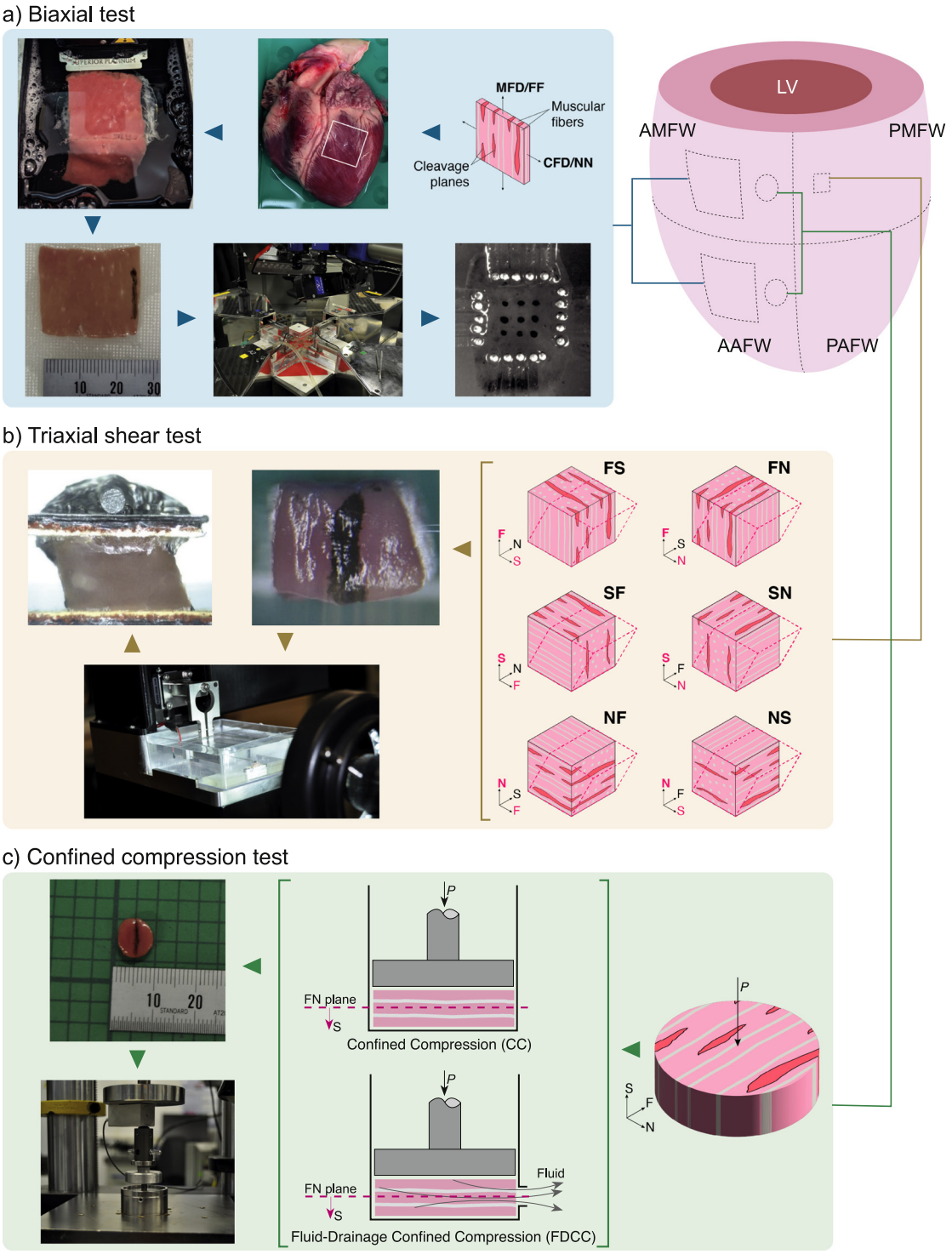

Fig. 1. (a) Biaxial extension testing procedure: (i) sample microstructure and alignment; (ii) first transmural cut performed, not yet parallel to MFD and CFD; (iii) vibratome cutter experimental set-up; (iv) 25 × 25 × 1 mm biaxial sample after preparation; (v) experimental set-up of the biaxial tests (black line indicates MFD direction); (vi) biaxial sample during mechanical testing. (b) Triaxial shear testing procedure: (i) different shear configurations regarding load orientation and the orthotropy directions; (ii) 4 × 4 × 4 mm shear specimen after processing (black line indicates F direction, and the other in-plane direction corresponds to N); (iii) experimental set-up of the triaxial shear tests; (iv) triaxial shear sample during mechanical testing. (c) Confined compression testing procedure: (i) sample microstructure and alignment; (ii) Confined Compression (CC) and Fluid-Drainage Confined Compression (FDCC) testing configuration; (iii) compression sample after preparation; (iv) experimental set-up of the compressive tests.

2. Materials and methods

2.1. Animals

We used porcine animal model as it is one of the most used in cardiovascular mechanics due to its close resemblance to the human heart. Porcine left ventricular transmural biopsy specimens (Fig. 1) were obtained from 13 white pigs (Sus scrofa domesticus) of 18-22 weeks of age (about 4 months old, 4MA) with a mean weight of 61.62 ± 5.65 kg. 5 extra animals were also used with different age, 36-42 weeks (about 8 months old, 8MA) with a mean weight of 121.36 ± 28.21 kg. All hearts were obtained at the

Table 1
Summary of mechanical tests for all the specimens. AMFW stands for antero-medial LV free wall, AAFW stands for antero-apical LV free wall, PMFW stands for postero-medial LV free wall. 4MA stands for 4 months old animals and 8MA stands for 8 months old animals.

Animal	Animal weight [kg]	Biaxial (AMFW)	Biaxial (AAFW)	Shear (PMFW)	Compression
4MA-1	62.8	3	–	6	–
4MA-2	54.5	3	–	6	–
4MA-3	54.9	2	–	7	–
4MA-4	53.4	2	–	6	–
4MA-5	64.1	2	–	7	–
4MA-6	64.0	2	–	6	–
4MA-7	59.5	2	–	7	–
4MA-8	62.0	1	4	–	13
4MA-9	61.6	2	4	–	18
4MA-10	61.0	1	5	–	28
4MA-11	70.0	1	4	–	25
4MA-12	60.2	–	5	–	14
4MA-13	73.0	3	2	–	14
Total 4MA	**–**	**24**	**24**	**45**	**112**
8MA-1	94.0	–	3	8	22
8MA-2	96.0	–	2	11	21
8MA-3	124.7	–	3	11	22
8MA-4	129.3	–	4	7	16
8MA-5	162.8	–	5	8	20
Total 8MA	**–**	**–**	**17**	**45**	**101**

Experimental Surgery Service of the Aragon Health Sciences Institute. Animals were cardioplegically arrested under deep anaesthesia with propofol (intravenous administration, up to 6 mg/kg) and inhaled sevofurane (1.9%) and sacrificed. Hearts were maintained in cold cardioplegia from extraction during transport to the laboratory (less than 2 h). All animal experiments complied with the regulations of the local animal welfare committee for the care and use of experimental animals and were approved by local authorities (Ethics Committee on Animal Experimentation, CEAEA, of the Aragon region, reference code PI36/20). All animal procedures followed the guidelines from Directive 2010/63/EU of the European Parliament on the protection of animals used for scientific purposes. Two different solutions were used during the sample obtention procedure: Tyrode's solution: composition in mM, NaCl 140, KCl 6, CaCl2 0.9, MgCl2 (.6H2O) 1, glucose 10, HEPES 10, supplemented with 30 mM 2, 3-butanedione monoxide (BDM) to inhibit contractile activity, pH adjusted to 7.4, all chemicals from Sigma Aldrich. Cardioplegic solution: 5.5 mM glucose, 0.5 mM MgSO4.7H2O, 24 mM KCl, 20 mM NaHCO3, 109 mM NaCl, 0.9 mM NaH2PO4 and 1.8 mM CaCl2, pH 7.4, all chemicals from Sigma Aldrich.

2.2. Biaxial testing

Specimen preparations. Left ventricular transmural tissue blocks (surface area 38×38 mm, 1.a) were cut with a single edge razor blade. To compare different regions of the LVFW, biaxial samples were obtained at two distinct locations. As will be detailed later, triaxial shear tests and confined compression tests were performed simultaneously with the biaxial tests. To ensure that myocardium was maintained in near physiological conditions, only two types of simultaneous tests were feasible per animal. In 7 animals, samples were obtained at the Anterior-Medial part of the LV Free Wall (AMFW) while at the remaining 6 animals, samples were obtained both at the Anterior-Apical area of the LV Free Wall (AAFW) and the AMFW region. A total of 24 samples were tested both at the AMFW and the AAFW (Table 1). The medial area was approximately one-third of the total ventricle length below the base, situated roughly 10-20 millimeters lower. The apical zone was chosen as close as possible to the ventricular apex to analyze the area where the fiber orientation is more dispersed (1). Tissue blocks were directly glued onto the vibratome cutting stage, mounting them epicardium-side down to ensure maximum longitudinal alignment of muscle fibers with the slicing plane (Fig. 1a) [51–53] and to minimize the number of fibers transected during sectioning, as myocardial fascicles primarily orient parallel to the epicardium [24,54,55]. 1 mm-thick slices were cut in freshly prepared ice-cold pre-oxygenated Tyrode's solution employing a high precision vibratome, advancing at a low speed of 0.04 mm/s and oscillating at an amplitude of 2 mm and a vibration frequency of 80 Hz. Calibration was performed before slicing each tissue block to ensure less than than 0.5 µm out-of-plane blade deviation. Every endocardial trabecular layer and area of gross chordae tendineae from papillary muscles was trimmed. Hence, samples ranged from sub-endocardium to sub-epicardium. After slicing, sections were maintained in cold cardioplegic solution until used for mechanical testing within the following 72 h. In all tests, we analyzed whether there was any impact on the mechanical response over this time due to the loss of physiological conditions. No significant difference was observed within the 72-hour timeframe. From these slices, squared specimens (25×25 mm) were prepared using a square cutter, with one side aligned with the mean-fiber direction, MFD, and the other with the cross-fiber direction, CFD, which corresponds to FF and NN following LeGrice FSN coordinate system, respectively (Fig. 1a). Nine dot markers were painted onto the specimens for later obtention of the real samples stretches (Fig. 1a). In Table 1, a summary of the tests performed is shown.

Biaxial extension protocol. Tests were performed using a true biaxial testing equipment (Instron Planar Biaxial Soft Tissue Test System, Fig. 1a) with a 10 N loading cell following the protocol presented by Sommer et al. in 2015 [28]. Four different stretch levels were consecutively applied (5-20% in 5% increments), with 4 preconditioning cycles and 1 measuring cycle at each stretch to get a steady response. The literature suggests a total of 5 to 10 cycles to achieve a steady response [18,20,21,23], but Sommer et al. asserted that 5 levels are sufficient [28]. Several loading ratios between MFD and CFD were considered at each stretch level (1(MFD):1(CFD), 1:0.75, 1:0.5, 0.75:1, 0.5:1) to capture the direction-dependent material response. A 2 mN equibi-

axial preloading was applied in all tests under quasi-static conditions (v=2 mm/min). To prevent cell contraction, samples were immersed in cardioplegia solution at body temperature (37° C). The Cauchy stress (σ) was obtained for the evaluation of the mechanical response. For an imcompressible material such as myocardium, Cauchy stress can be determined as:

$$\sigma_{ii} = \lambda_i P_{ii} = \lambda_i \frac{F_{ii}}{tL_j} \tag{1}$$

where $\lambda_i = x_i/X_i$ represents tissue stretch in each direction (MFD and CFD), based on the dimensions of the loaded (x_i) and unloaded (X_i) configuration; P_{ii} refers to the first Piola-Kirchhoff stress in each direction; F_{ii} corresponds to the normal forces in each direction (ii does not stand for summation); t is the specimen thickness in the unloaded reference configuration (1 mm) and L_j are the transverse-to-the-force lengths of the sample sides in the undeformed state (which were about 20 mm in every specimen). To monitor the real sample deformations and consider potential shear strains, nine dots were marked at the central part of the biaxial sample using waterproof marker. Images were captured at a frequency of 2 Hz, and shear strains and stresses were computed as described in [56].

2.3. Triaxial shear testing

Specimen preparations. Due to the laminar architecture of the myocardium [24], a right-handed orthogonal set of axes was established regarding the fiber spatial distribution along the ventricle wall: the myofiber direction or fiber axis (F), which correspond to MFD at biaxial testing; the direction transverse to the fiber axis within the layer or sheet axis (S); and transversal direction to both of them (N), which corresponds to CFD. These directions lead to six different shear configurations (Fig. 1b). To guarantee a homogeneous fiber orientation within the sample, the cubic specimen should be as small as possible. 4 mm cubic samples aligned to local axes (FSN) were manually cut with a vibratome blade (Fig. 1b). For easier structural identification, Evans blue dye was used to highlight the laminar structure. As the AMFW region was entirely dedicated to biaxial and compressive testing, shear samples were obtained at the Posterior-Medial area of the LV Free Wall (PMFW), as close as possible to the biaxial cut (Fig. 1b). We did not observed structural differences between AMFW and PMFW samples. The specimen was then glued to both the bottom and upper specimen holders of the testing device, using sandpaper to improve holders' attachment. In Table 1 we show a summary of the preformed experiments.

Triaxial shear protocol. Triaxial shear tests were conducted using a multiaxial testing device (CellScale MicroTester G2, Fig. 1b) following the protocol presented by Dokos et al. in 2002 [27]. Five different stretch levels (10-50% in 10% increments) were applied consecutively, with two preconditioning cycles and one measuring cycle for each level. Only one shear mode was evaluated for each sample. A total of 45 samples were tested, and all six shear modes were performed for all animals (Table 1). Equally to biaxial testing, all tests were performed at quasi-static conditions (v=2 mm/min) and immersed in cardioplegia solution at body temperature (37°C) to prevent cell contraction. Once again, all tests were performed within 72h after heart extraction. The amount of shear (γ_{ij}) and shear stresses (τ_{ij}) for each shear configuration (referred as 'ij') was obtained to quantify the shear response of the tissue as:

$$\gamma_{ij} = \frac{\Delta L}{L_i}; \qquad \tau_{ij} = \frac{F_j}{L_i L_k} \tag{2}$$

where ΔL denotes the shear displacement and L_i, L_j and L_k are the dimensions (along F, S and N, respectively) of the cubic sample as described at Fig. 1b (which were about 4 mm in all the specimens); F_j refers to the recorded shear force.

2.4. Compression testing

Specimen preparations. As illustrated in Fig. 1, compression samples were also obtained from parallel-to-the-epicardium slices, simultaneously to biaxial samples. Samples were obtained both from the AMFW and the AAFW regions. In this case, 2 mm thick 38 × 38 mm slices were obtained with the vibratome cutter, maintaining the cutting procedure of the biaxial specimens. Samples also ranged from sub-endocardium to sub-epicardium to address variations in compressibility across the transmural thickness of the LVFW. Three discrete thickness levels where distinguished, sub-epicardium (SEpi), up to 3 mm below the epicardial surface; sub-endocardium (SEnd), up to 3 mm over the endocardial surface and myocardium (MIO), which corresponds to the rest of the wall. From these slices, cylindrical samples of 6 and 8 mm of diameter were prepared so that the circular section coincides with the FN plane and the transverse plane. Thus, the compression load takes place along the S direction (Fig. 1c).

Confined compression protocol. Two different confined compression tests were conducted. In the first one, the tooling had a small exit orifice which acted as a fluid drainage (Fluid Drainage Confined Compression, FDCC). In the second one, no drainage was considered so the sample was fully confined (Confined Compression, CC). Both tests followed the protocol presented by McEvoy et al. [37]. A total of 112 confined tests were performed, in which 52 were CC tests and 60 FDCC tests (Table 1). Briefly, specimens were placed into a rigid die with its same transversal dimensions. Compression was imposed using a uniaxial machine (Instron MicroTester I5848 with a 500 N loading cell, Fig. 1c) under quasi-static conditions (v=2 mm/min). In both CC and FDCC tests, two loading stages were applied. First, a volumetric compression stage was applied until the specimen was deformed to a volumetric strain of 10%. As the compression is confined, axial strain is equal to volumetric strain. Then, a fluid drainage stage was applied in which the indenter is maintained during a certain time (15 min) to allow the fluid to exit the sample. Of course, fluid was only able to come out in the FDCC tests. All tests were performed within 72h after heart extraction. The volumetric strain (J) and hydrostatic stress (P) were obtained as:

$$J = \frac{\Delta V}{V_0}; \qquad P = \frac{F}{\pi r^2} \tag{3}$$

where ΔV is the volumetric variation associated with compression, V_0 the original volume, and r the radius of the sample, which was 4 mm for CC and 3 mm for FDCC. Table 1 provides a summary of the tests performed.

2.5. Histological analysis

In order to analyze the tissue microstructure at the different sample locations and age groups, a histological analysis was carried out. We aimed to analyze the spatial distribution of the main microstructural components from a mechanical standpoint, and to relate its distribution with the observed mechanical response. Sample processing was performed at the Central Anatomical Pathology Unit of the Aragon Health Sciences Institute. Formaldehyde-fixed samples were processed in cassettes using an automatic tissue processor (Tissue-Tek Xpress x50). Then, the tissue blocks were made with Leica EG1150 unit, after which they were solidified on a cold plate. Paraffin-embedded samples were cut into 3 µm thick sections (Leica RM2255 rotary microtome) and kept in a tempered bath. Then, they were collected with superfrost plus slides (Bio-optica. Labolan Ref. 50559). Slides were placed on vertical racks and left to dry overnight at 37°C, then a deparaffinization and hydration process was carried out. Subsequently, the sections were stained with Picrosirius Red staining (PR), Masson's Trichrome

staining (MT) and Hematoxylin-Eosin staining (HE) to capture muscular and collagenous fibers distribution. After staining, the sections were dehydrated by immersion in ascending alcohol solutions (70%, 96% and 100%) for 15s each. Finally, all sections were cleaned with xylene for 15s and mounted on the Leica CV5030 automatic mounter using Epredia glass coverslips.

2.6. Influence of samples location on the mechanical response

As mentioned earlier, in addition to characterizing the overall myocardium response, two additional studies were conducted: in the first one, the variation of the mechanical properties was investigated as a function of the sample's position, and in the second one, the influence of age on the mechanical response was examined. Within the location analysis, various comparisons were made, all performed on animals of the same age group (4MA). First, we examined the properties along the longitudinal direction of the LVFW. Two different regions along that direction, AAFW ($n = 44$) and AMFW ($n = 68$) were studied. All samples were collected from the central part of the myocardium thickness. No location analysis was conducted for the triaxial shear tests, as all samples were obtained from the same zone (PMFW). A second analysis was conducted to assess the variation of the tissue response along the transmural thickness of the wall, ranging from sub-endocardium to sub-epicardium. In this second analysis all samples were collected at the AMFW region and at least 17 samples were considered in each region.

2.7. Influence of animal age on the mechanical response

As mentioned, to evaluate the influence of age on tissue response, experiments were conducted on an additional set of 5 animals at 8 months of age (8MA), where the weight of the animals was approximately double that of the 4MA animals. The weights per animal for each individual tested are listed in Table 1. The same mechanical tests mentioned above (biaxial, triaxial shear, and CC/FDCC compression tests) were conducted for this second group, as described in Table 1.

2.8. Statistical analysis

Statistical analyses were conducted to assess correlations between different data groups. Pearson's correlation coefficient was used for continuous samples, such as the evolution of peak stresses concerning animal weights. Additionally, statistical differences in mechanical properties between regions or age groups were also examined. The Shapiro-Wilk test was employed to assess the normality of results within each subgroup. Depending on the normality of each data group, p-values were determined using Student's t-distribution for normal samples and Mann-Whitney U-distribution for non-normal samples, considering $p < 0.05$ as significant. Statistical analyses were performed using a custom Matlab R2024a program. All data values are presented as mean ± standard deviation (SD).

3. Results

3.1. Biaxial extension tests

In Fig. 2, we present a summary of the results from the true biaxial characterization. All plots show Cauchy stress vs. stretch results. We have considered the results from AMFW region in 4MA animals as reference, and we have kept the results for AAFW and 8MA animals for the specific analyses described later. Although a relevant viscoelastic behavior is noticeable, this study will focus solely on the elastic part of the response. Myocardial tissue exhibits a highly non-linear and anisotropic response, with higher stiffness in the MFD (FF) direction than in the CFD (NN) one, as expected. Fig. 2a, illustrates the characteristic preconditioning behavior (specimen 4MA-2-2) under equibiaxial loading at 10 and 15% of stretch, which was reproducible across other animals and stress levels. The results suggest that the imposed preconditioning is sufficient to reach a steady state, as the response stabilizes from the second or third cycle. It was observed that in practically all samples the shear stresses were negligible (less than 5%), but even so they were accounted to obtain the actual normal stress. In the few samples where relevant shear stresses were obtained due to suboptimal sample placement, the experiments were discarded, and they have not been included in the study nor in the summary shown in Table 1.

Fig. 2 b shows the measuring cycle of the equibiaxial results at each stretch level (1.05 to 1.20, in 0.05 increments) for a representative sample (specimen 4MA-2-2). These graphs show evidence of softening effects in the myocardial tissue, with a progressive reduction in stiffness as the maximum strain is imposed and maintained over time. Fig. 2c presents the representative response for all loading ratios applied at 10% stretch. The different loading ratios remain consistent with the Poisson effect, as we observed in both directions a progressive increase in stiffness, consistent with the state of deformation in the transverse direction. We also observe some cross-coupling effect as the stiffness in both directions varies depending of the load in the transverse direction.

Although the selected specimen is representative of the global response, assessing average results to understand inter-patient variability is also convenient. In Fig. 2d, averaged equibiaxial curves ($n = 24$) are organised by stretch level, while Fig. 2e shows all the averaged loading ratios curves at 10% of stretch. We did not include the deviation in Fig. 2e, for the sake of clarity, but it was comparable to the one shown in Fig. 2d. Although some variability does exist between different animals, as represented by the standard deviation, the overall trend is evident and aligns with the explanations in the previous plots. Table 2 also collects the peak Cauchy stress for both MFD and CFD. Once again, higher peak stress is observed in MFD, resulting in an anisotropy ratio ($\frac{P_{MFD}}{P_{CFD}}$) around 2 for all cases (1.96-2.40), which is in good agreement with values reported in the literature (between 1.5 and 3) [18,20,22,28].

Table 2
Average peak equibiaxial stress both in MFD (which corresponds to FF) and CFD (which corresponds to NN), and anisotropy ratio at every imposed stretch level.

	5% of strain	10% of strain	15% of strain	20% of strain
MFD (kPa)	4.64 ± 0.86	8.35 ± 1.43	11.24 ± 1.89	13.23 ± 2.55
CFD (kPa)	2.03 ± 1.69	3.95 ± 1.69	6.07 ± 1.43	7.92 ± 1.60
MFD/CFD (-)	2.14	2.40	1.99	1.96

3.2. Triaxial shear extension tests

In Fig. 3, the results obtained from the triaxial shear characterization are presented. All plots depict Cauchy stress vs. amount of shear. Again, triaxial shear results exhibit a highly non-linear response, with a significant viscoelastic component. Besides, softening is also visible in these plots. Fig. 3b shows a global comparison of the six different shear configurations at $\gamma = 0.5$, while Fig. 3a,c,e display the results for all the applied shear levels (0.1 to 0.5) separated by shearing planes (F-S-N) for clearer understanding. All these plots present the results for a representative specimen (4MA-4). The myocardium presents an evident orthotropic response, which can be differentiated into three different groups. First, tests where the shear stress is mainly absorbed by the F

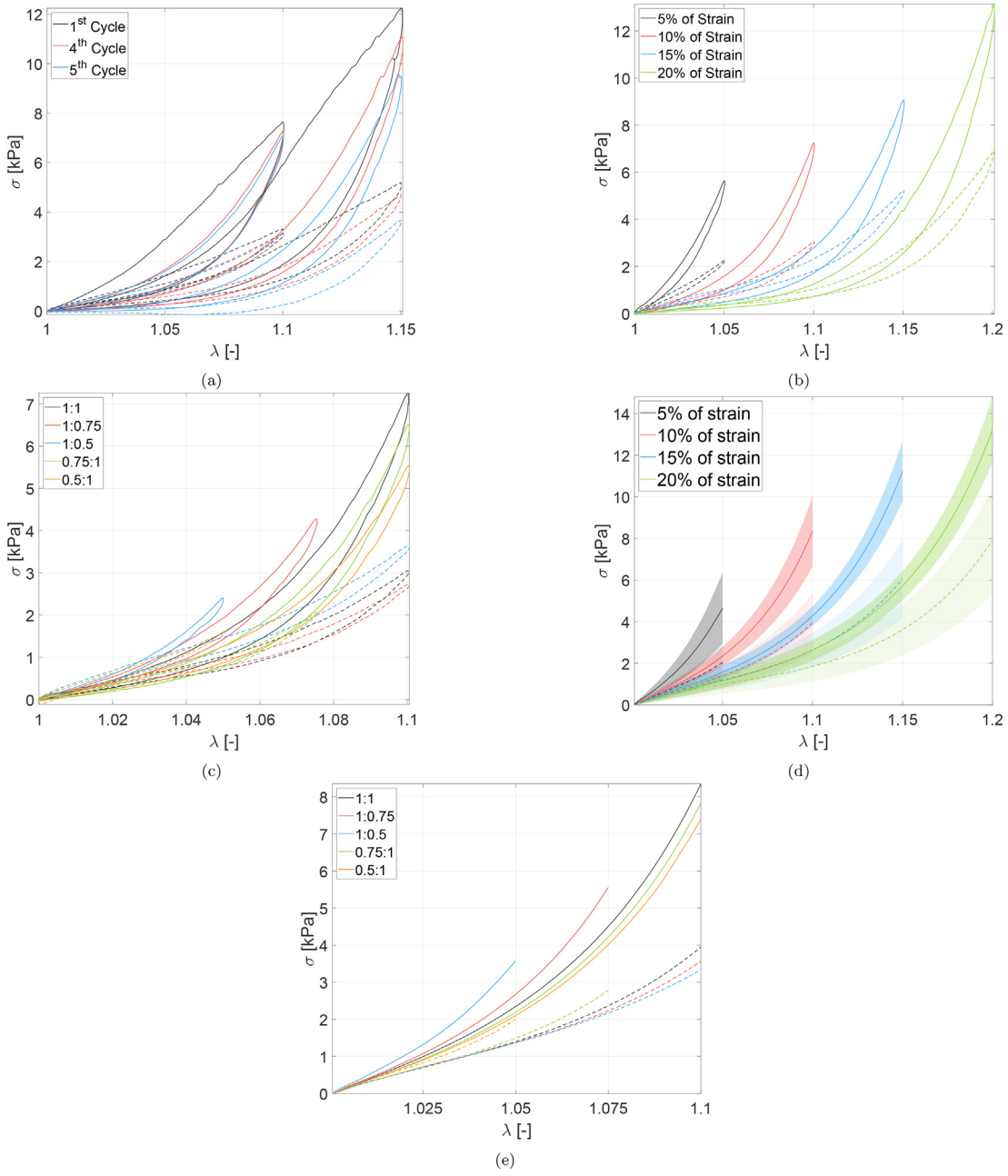

Fig. 2. Biaxial results for a representative specimen (specimen 4M-2-2) and biaxial average results. In all plots, solid line refers to MFD and dashed line to CFD. (a) Typical preconditioning behavior at two strain levels (10 and 15%). (b) Representative equibiaxial results at the measuring cycle for all imposed strain levels (5, 10, 15 and 20%). (c) Representative results for all the imposed loading ratios at 10% of stretch. (d) Equibiaxial average results ($n = 24$) for all imposed strain levels; the standard deviation of each curve is shown as a shaded area. (e) Averaged results ($n = 24$) for all the imposed loading ratios at 10% of stretch; the deviation is not shown here for the sake of clarity due to the high number of curves in the same plot.

direction (FN-FS) show the stiffest response at all strain levels (around 8 kPa for $\gamma = 0.5$). Then, those where the shear stress is mainly in the S direction (SF-SN) show intermediate stress values (around 5 kPa for $\gamma = 0.5$). Finally, those in which the shear stress falls mainly on the N direction (NF-NS) present the most compliant response (around 3 kPa for $\gamma = 0.5$). This is consistent with several results in literature [27,28,31,33].

In Fig. 3d, the characteristic preconditioning behavior is illustrated (specimen 4MA-4) at 40% and 50% of shear stretch. As described in [27,28], only 2 instead of 4 preconditioning cycles are needed in shear tests. We corroborated that the myocardial tissue is able to reach a steady state even after a single preconditioning cycle.

Fig. 3 f presents the average peak stresses in all shear configurations for γ=0.5 (a total of 45 samples were tested, and at least $n > 8$ in each shear modes). Again, the average response shows an orthotropic behavior, with a progressively increasing stiffness along the N-S-F directions, respectively. There are small differences between the values obtained in γ and -γ, which may be associated with small heterogeneities in the shape of the samples that give rise to asymmetries. Although still reasonable, they were particularly evident in FS. In both directions, the orthotropy of the tissue is evident. The deviation obtained is in an acceptable range, although FS test shows a slightly higher value. Inter-specimen variation is usually attributed to differences in tissue architecture, collagen density and fiber dispersion along the FSN direc-

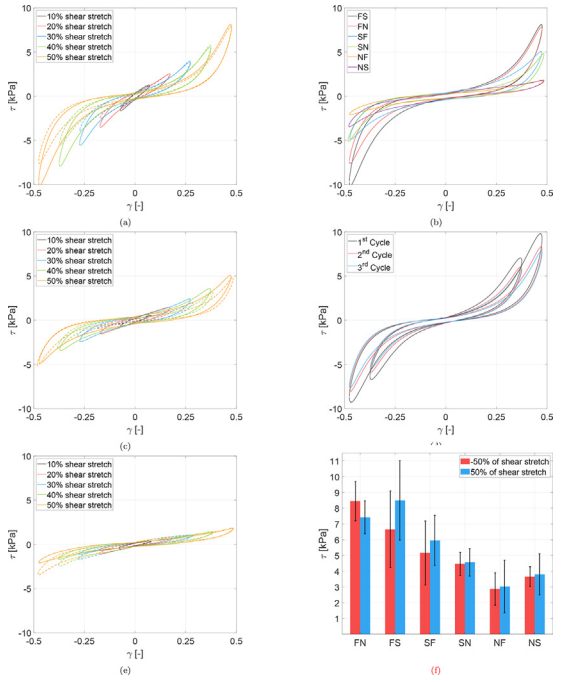

Fig. 3. Results for a representative specimen (specimen 4M-4) and average results for the tangential tests. (a)-(c)-(e) Representative results of the last cycle at each shear stretch level for FS(solid)-FN(dotted), SF(solid)-SN(dotted) and NF(solid)-NS(dotted), respectively. (b) Representative results of the last cycle at 50% shear stretch for all strain modes. (d) Representative preconditioning response at two different stretch levels (40 and 50%) (f) Averaged peak stress values ($n = 45$) for all strain modes at 50 and -50% shear stretch.

tions [27,28], but the general trends were similar for the different animals.

3.3. Compression tests

The results of FDCC and CC tests are shown in Fig. 4. The CC tests primarily characterize the inherent incompressibility of the tissue, while FDCC tests provide insights into the tissue's permeability and its resistance to fluid movement, such as blood flow during ventricular perfusion. Despite both tests were conducted with the the same protocol (see Section 2.4), distinct results were obtained. Fig. 4a shows the global response for the CC tests (black line). A detailed discussion on local results is performed below. Although the tissue was perfused and completely confined, it exhibited some degree of compressibility, with volumetric variations up to 10% for stress values of 3-4 MPa, which is significantly higher than the typical stiffness recorded in other mechanical tests. This compressibility can be attributed to the cutting and handling during sample extraction, allowing some fluid to leave the tissue before the start of the test. In FDCC tests (Fig. 4b), the global response present significant lower stresses due to fluid drainage, with a 2-orders of magnitude reduction compared to the FDCC (approximately 30-40 kPa). The response stabilizes at around 300-400 s, well before the test's conclusion ($t = 900$ s), suggesting that the steady state situation was achieved. At the end of the second phase, a zero-stress state is not reached, but the remaining stress values are almost negligible (3-4 kPa).

3.4. Histological analysis

Fig. 5 shows the results of the histological analysis employing three distinct stains to analyze the distribution of both muscular and collagenous fibers. PR staining facilitates collagen fiber visualization, with collagen-I appearing in yellowish and reddish tones under polarized light, and collagen-III in greenish tones. TM staining accentuates muscle tissue in reddish tones and collagen-I in bluish tones. Meanwhile, HE staining exclusively enables the analysis of muscle fiber distribution, coloring them in reddish or pinkish tones, with cell nuclei visible in blue-violet. All staining procedures were conducted on biaxial samples post mechanical testing. Since the area shown is very small (around 650×500 µm), we carefully checked that it was representative of the tissue in each of the regions. All images correspond to the central depth of the myocardial wall. We also analyzed the differences between the central area with respect to the samples closer to the sub-endocardium and sub-epicardium, but no significant differences in tissue structure were found, so they have not been included.

The four groups of images represent both areas considered (AMFW and AAFW) across the two age groups analyzed (4MA and 8MA). Focusing first on the AMFW zone of the 4MA animals (Fig. 5a), both MT and HE staining demonstrate a well-defined preferential alignment of muscle fibers (indicated in Fig. 5 as MFD), which are organized into parallel layers separated by cleavage planes, as described by LeGrice [24]. In these cleavage planes, collagen-I fibers appear in blue in TM staining and much more clearly in red and yellow stripes in PR staining. However, a large distribution of collagen fibers is not observed, since in PR only thin stripes appear between the muscle fiber layers and are almost imperceptible under TM.

In the AAFW zone of the same animals (Fig. 5b), the tissue structure is quite similar to the AMFW zone. Here, too, a modest distribution of collagen fibers is observed, mainly in PR staining. Notably, a disparity in fiber alignment becomes apparent, with muscle fibers exhibiting a less homogeneous orientation compared to the AMFW, as observed through HE and TM staining. This trend is also maintained in the 8MA animals.

Similar trends persist in 8MA, wherein AMFW (Fig. 5c) also exhibits greater alignment compared to AAFW (Fig. 5d). When comparing 8MA to 4MA, substantial changes in tissue structure emerge. At 8MA we observe a greater density of muscle tissue, with a greater number of fibers between cleavage planes and greater packing between them (TM and HE). In addition, the amount of collagen fibers also increases, with a higher density of collagen-I at 8MA through PR staining that is now even visible with TM. These structural modifications correspond to discernible mechanical disparities observed in 8MA animals, as will be elaborated subsequently.

3.5. Influence of sample location on the mechanical response

3.5.1. Differences between the AAFW and the AMFW regions

Equibiaxial tests. Fig. 6a–c show the equibiaxial results for the 4MA animals at AMFW (black) and AAFW (blue), as well as the anisotropy ratio. Looking at the mean values, the AAFW zone ($n = 24$) shows a slightly less stiff response, reaching peak stresses of 6.31 and 3.36 kPa (MFD and CFD) with respect to the values of 8.36 and 3.97 in the AMFW zone ($n = 24$). This results in a reduction of 24.58% and 14.21% in each direction, respectively. In terms of the anisotropy, the anisotropy ratio is reduced from 2.40 to 2.12. According to the statistical analysis, we can consider a significant variation at the MFD direction ($p = 0.016$) but not in CFD nor the anisotropy ratio ($p > 0.05$). This suggest that the behavior of the tissue may not be homogeneous from the AMFW to the AAFW, at least along the MFD. These minor variations may be related to differences in the architecture of muscle fibers in these two regions. As shown in Fig. 5, in AMFW, the alignment of FSN directions is fairly homogeneous, albeit with some dispersion. However, in the AAFW region, the degree of fiber alignment is significantly lower due to the ventricle's geometry. Consequently, a more isotropic and slightly less rigid response is observed for the AAFW area.

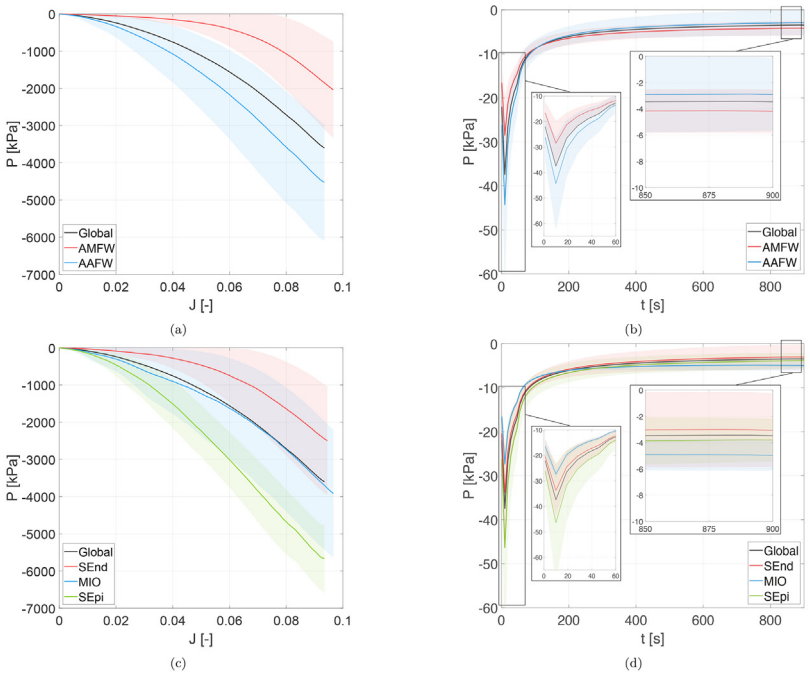

Fig. 4. Compression test results for 4M animals both globally and locally. (a) CC test results divided between global ($n = 52$), medial ($n = 18$) and apical ($n = 34$). (b) FDCC test results divided between global ($n = 60$), medial ($n = 26$) and apical ($n = 34$). (c) CC test results divided between global, sub-endocardium, myocardium and sub-epicardium. (d) FDCC test results divided between global, sub-endocardium, myocardium and sub-epicardium. Solid line stands for mean results and shaded area shows the standard deviation.

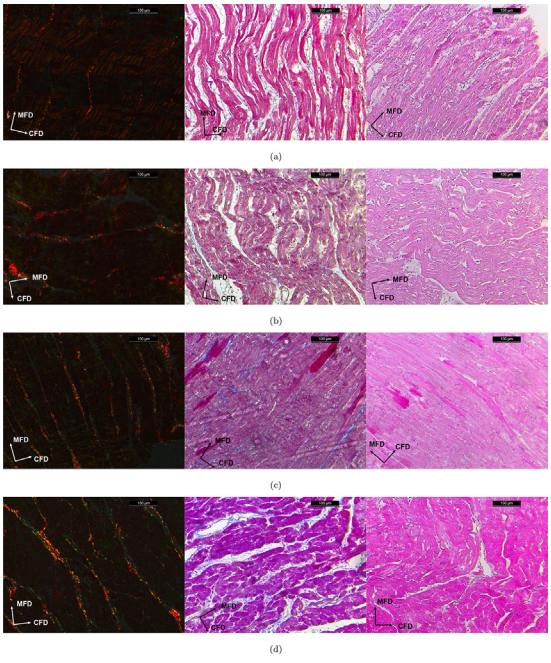

Fig. 5. Results of the histological analysis. (a) 4MA animals at AMFW region; (b) 4MA animals at AAFW region; (c) 8MA animals at AMFW region; (d) 8MA animals at AAFW region. For all plots, we show Picrosirius Red staining under polarized light (PR, left), Masson's Trichrome staining (MT, center) and Hematoxylin-Eosin staining (HE, right). Global Main and Cross Fiber Directions are indicated as MFD and CFD for each image.

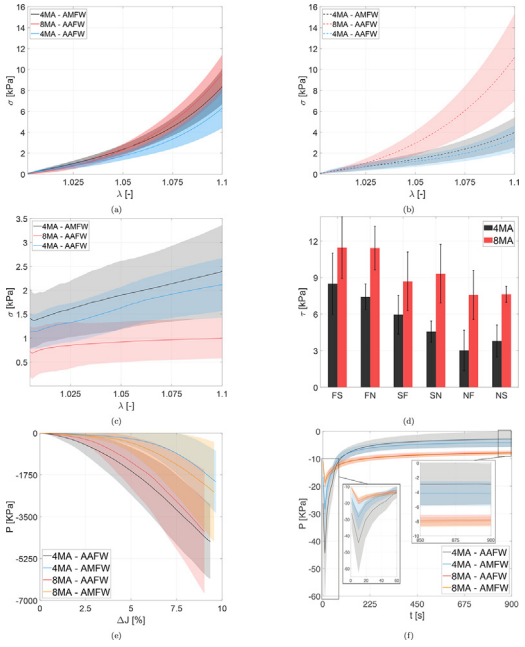

Fig. 6. Influence of age on the mechanical response. Variation of the equibiaxial response in (a) MFD, (b) CFD and (c) the anisotropy ratio. (d) Variation of the triaxial shear response in all the strain modes. (e) Variation of the compressibility of the tissue in CC tests. (f) Variation of the compressibility of the tissue in FDCC tests. In c and d, solid line stands for mean results and shaded area shows the standard deviation.

Compression tests. The variation between the AMFW and the AAFW zones is shown in Fig. 4a,b. Notably, in CC tests, a significant disparity is visible between both zones, evidencing considerably higher incompressibility in the AAFW zone ($n = 34$) compared to the AMFW zone ($n = 18$). Despite dispersion is elevated in both groups, the responses are distinctly separated ($p = 2.12e\text{-}7$), and the deviation ranges between the two groups do not overlap. In the FDCC tests, a much more uniform response is obtained between the two zones, with highly comparable results ($n = 34$ for AAFW and $n = 26$ for AMFW). Upon closer inspection, minor lo-

Table 3
Variation of the 8MA peak stresses respect the 4MA animals in all the considered loading paths.

FF (MFD)	NN (CFD)	FS	FN	SF	SN	NF	NS
45.56%	216.63%	25.07%	53.78%	45.89%	111.47%	150.45%	91.33%

Table 4
Pearson correlation coefficients (R) and p-values (p) between the peak stresses along MFD, CFD and anisotropy ratio (AR) and the two considered variables (normalised radial coordinate, $\bar{r}$, and animal weight, w).

Parameter	σ_{MFD}^{max}	σ_{CFD}^{max}	AR
$R_{\bar{r}}$	0.109	0.169	0.023
$p_{\bar{r}}$	0.678	0.517	0.932
R_w	0.354	0.729	−0.573
p_w	0.106	5.09e-9	4.36e-5

cal differences appear in the maximum values reached at the end of volumetric compression, as well as in the final stress value after the fluid drainage phase. However, although these small differences do exist, there is no statistical significance ($p > 0.05$ in all cases).

3.5.2. Differences along the transmural thickness

Equibiaxial tests. In addition to the differences between AMFW and AAFW, we have also analyzed the mechanical response along the transmural thickness. We have examined its correlation with the peak stress along both MFD and CFD, as well as the anisotropy ratio of all the recorded samples as presented in Table 4. We used Pearson's linear correlation coefficient, although we also tested non-linear coefficients such as Kendall's or Spearman's, obtaining the same results. Our results demonstrate that there is no appreciable dependence between the considered variables, indicating that the mechanical properties can be considered homogeneous throughout the ventricular thickness ($p > 0.05$ in all combinations). This finding aligns with previous observations [20,28,34].

Compression tests. Regarding the compression tests, as mentioned earlier, samples were not obtained along the entire thickness of the myocardium. Instead, samples were grouped into three discrete groups of thickness levels (SEnd, $n = 61$; MIO, $n = 17$; and SEpi, $n = 34$). Once again, CC tests (Fig. 4c) revealed significant differences between the three zones ($p < 0.014$ in all combinations), with incompressibility gradually decreasing as we approach the endocardial surface ($SEnd < MIO < SEpi$). The results of FDCC tests (Fig. 4d) are again very similar to each other, with only minor differences in the maximum values at the end of the two differentiated phases and no statistical significance ($p > 0.05$ in all cases).

3.6. Influence of animal age on the mechanical response

Equibiaxial and triaxial shear tests. Fig. 6a–d show the results of the equibiaxial and triaxial shear tests for the 4MA and 8MA animals. Except for FS in STS ($p = 0.12$), in all tests a substantial stiffening is visible ($p < 0.028$ in all cases), as the maximum stress level reached in all deformation modes increases. Table 3 shows the percentage increase in the maximum stress for each deformation mode of the 8MA animals with respect to those of the 4MA animals. In all modes, an increase of at least 25.07% is observed, with a significantly higher increase in SN, NF, NS, and NN (CFD) compared to the others. This phenomenon may be related to microstructural changes as will be discussed below. Similar to the transmural thickness, we also determined the correlation between the weight of the animal and its more representative mechanical results by means of Pearson's coefficient (Table 4). The results indicate a weak, statistically insignificant dependence of the peak MFD stress ($p = 0.1059$), and a more pronounced ascending dependence for CFD ($p = 5.09e\text{-}9$). Consequently, there is a strong decreasing correlation for the anisotropy ratio ($p = 4.36e\text{-}5$), suggesting that samples from heavier animals exhibit a more isotropic behavior.

Compression tests. Fig. 6e–f depicts the comparison between the 4MA and 8MA results for both CC and FDCC in the AMFW and AAFW zones. As mentioned, CC results show a strong dependence with the location of the sample. However, when examining the same zone at both ages, the results for the 4MA and 8MA are similar, indicating that the CC response varies only with the sample's location, not with animal age ($p > 0.68$ in both areas). Regarding the FDCC tests, a strong dependence on the age of the animals is observed, with significant differences between the 4MA and 8MA animal groups ($p < 6.36e-7$ in all cases). Nevertheless, the results between the two locations analyzed were practically identical for a given age. The FDCC results of the 8MA groups showed lower stress values at the end of volumetric compression, but the recovery after the fluid drainage phase was also much lower. All these findings indicate that the evaluated age gap does not affect tissue incompressibility but have a significant impact on tissue permeability and its resistance to fluid movement.

To gain further insight into the fluid evacuation capability, we also investigated the temporal variation of the hydrostatic pressure ($\dot{P} = dP/dt$) and the duration from peak compressive load to 90% depressurization (T90). Fig. 7 illustrates the maximum values

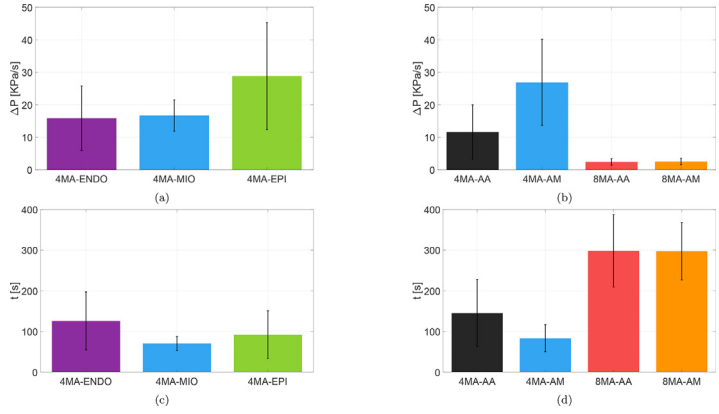

Fig. 7. (a) Peak hydrostatic pressure relaxation rate recorded in the FDCC tests, classified by radial coordinate and (b) by longitudinal coordinate as well as age group. (c) Transcurred time for a 90% depressurization (T90), classified by radial coordinate and (d) by longitudinal coordinate as well as age group.

of each parameter for all the analyzed groups. For 4MA, there was no significant variance radially ($p > 0.06$ in all cases), whereas longitudinally, the AAFW region displayed higher pressure variation ($p = 3.37e\text{-}6$) and faster T90 ($p = 0.0014$) compared to AMFW. This indicates a greater fluid evacuation potential in the apical region, possibly due to variances in vasculature between the two regions. Conversely, a notable decrease in $\dot{P}$ is evident in 8MA ($p < 6.57e\text{-}10$ in both areas), as well as an important increase in its depressurization time ($p < 6.36e\text{-}7$ in both areas), surpassing the variations observed in different areas of 4MA animals. This confirms that older animals tend to reduce its capacity to evacuate the stored fluid, likely attributable to microstructural tissue changes.

4. Discussion

4.1. True biaxial experiments

Myocardium exhibits a highly non-linear hyperelastic behavior, clearly anisotropic, being stiffer along the MFD (where myocytes predominate) than in the CFD. Additionally, a noticeable viscoelastic component was present, although this study focuses only on the elastic response. This non-linear hyperelastic behavior is commonly observed in soft tissues [57–61]. The average biaxial response shows a certain dispersion, typical of the inherent heterogeneity of biological tissues. Nevertheless, the observed trends at the individual level were consistently maintained from the sample standpoint. This not only confirms the generalizability of the conclusions drawn from these tests but also indicates the reproducibility of our methodology. We would like to point out that meticulous attention must be paid to the sample cutting, as we did observe a large variability in results when samples were not carefully obtained along the orthotropic directions of the tissue.

We did observe softening effects in our tests, obtaining lower stiffness for the same stretch levels as the loading peak stretch was surpassed. This phenomenon has been extensively reported in the literature when characterizing soft tissues [62–64], and its origin is not entirely clear. Various factors have been suggested, including the disruption of perimysial collagen due to excessive shearing between muscle layers [65,66], stretch-dependent damage on the endomysial collagen [67], changes in the collagen matrix where the myocytes are embedded [68], or disruption of intracellular structures such as myofilaments or cytoskeletal proteins [69–72]. Our results showed slightly greater softening effects than those presented by Sommer et al. [28]. Although the testing and sample treatment protocols were the same in both studies, we hypothesize that this difference may be related to variations in patient age between the two studies.

Our equibiaxial results have proven to be consistent to those in the literature. In terms of tissue anisotropy, we obtained a ratio of 2-2.4 between MFD and CFD, which aligns well with ratios reported in other equibiaxial studies for LV myocardium in canine specimens (1.5-3) [18,19], ovine myocardium (about 1.6) [22], human myocardium (about 2) [28], and murine myocardium (1-2.5) [30]. Focusing on equibiaxial Cauchy peak stresses in MFD-CFD at 10% stretch, great variability is observed in the literature. Values range from 0.8-0.6 kPa [18] and 1.2-0.8 kPa for canine myocardium [20], 2.0-1.3 kPa for ovine myocardium [22], 8.3-5.0 kPa for human myocardium [28], 4.0-2.0 kPa for murine myocardium [30], and 22.0-14.0 kPa for porcine myocardium [32]. We believe that these variations may be attributed to differences in the testing protocols and animal models used in each of them. Notably, some of these studies [18,20,30] do not differentiate between MFD and CFD but assume that these directions coincide with circumferential and longitudinal directions, respectively. Moreover, some of these studies [18,20] lack clear preconditioning criteria and do not provide averaged results. However, our results closely align with those presented by Sommer [28], while the differences with those in Ahmad [32] are small. Our study uses porcine myocardium, while these studies use human and porcine myocardium, respectively. Additionally, our protocol coincides with that used in their biaxial studies. This suggests that comparable protocols and animal models can yield reproducible results.

4.2. Triaxial simple shear experiments

As mentioned above, due to the orthotropic nature of myocardium [24,25], we conducted triaxial shear testing to complement biaxial information. We imposed different stretch levels ($\gamma = 0.1 - 0.5$), which fairly cover the range of shear deformations reported for the beating heart [27]. Our tests confirmed the highly non-linear orthotropic hyperelastic behavior of the myocardium (Fig. 3), which is well justified by the tridimensional fiber field described by LeGrice [24]. As detailed in Holzapfel & Ogden [25], the myocardial structure defines three principal directions: F, characterized by tightly packed groups of well-aligned cardiac myocytes; S, corresponding to the fiber sheets plane primarily composed of endomysial collagen fibers and thick coiled perimysial collagen fibers (which will be now referred just as 'endomysial' collagen) and N, which is normal to the FS plane and is mainly constituted by long perimysial collagen fibers that connect the muscle layers across cleavage planes (which will be now refereed just as 'perimysial' collagen). This structure is clearly translated to the triaxial shear response. FN-FS configurations exhibit the stiffest behavior as shear stress is predominantly absorbed by the myocytes (F). SF-SN tests reach the second-highest stress levels, with shear stress primarily absorbed by 'endomysial' collagen (S). Lastly, NF-NS configurations display the least rigid behavior, with shear stress predominantly absorbed by 'perimysial' collagen (N). This effect is shown in Fig. 1, where the directions that absorb the majority of the shear stress are highlighted for each configuration. This orthotropic response has been well-documented *in vitro* [27,28,31,33] and *in vivo* [73,74].

As in the biaxial tests, passive ventricular myocardium also exhibits strain softening under shear conditions. This phenomenon occurred across all the imposed deformation levels and could not be attributed to viscoelastic effects, as it remained stable over time. The softening effect was evident both for positive and negative shear stretch. Softening in shear testing has also been reported in multiple *in vitro* [27,28] and *ex vivo* [65,66] studies. As discussed in the biaxial experiments, softening is attributed to various mechanisms. Dokos et al. [27] observed softening at very low shear stretch values ($\gamma = 0.025 - 0.05$) and then discarded that it may be related to the disruption of connective structures due to excessive shear, such as endomysial or perimysial collagen fibers. Sommer et al. [28] also observed early softening effects and added that it may be due to a rearrangement of the extracellular connective tissue associated with altered mechanical loading. Our results are consistent with these latter statements as we also observed softening effects at low shear stretch values.

For a 40% shear stretch, the study by Dokos et al. [27] reported mean values of approximately $16 - 7.5 - 5$ kPa for porcine LV in the F-S-N directions, respectively, averaging across configurations within each group (e.g., FS and FN for F). Sommer et al. [28] obtained values of $4.25 - 2.75 - 2.25$ kPa for human myocardium. Kakaletsis et al. [31] reported $7.5 - 2 - 3.5$ kPa for ovine LV, although they show large asymmetries between positive and negative shear stretch and it is not entirely clear whether their protocol is the same as in Dokos', Sommer's or ours. We obtained values of $6.17 - 3.66 - 2.50$ kPa, which are comparable to the aforementioned studies. We did not include the study by Avazmohammadi et al. [33] due to their use of a different sample orientation which can not be directly compared with the others. When

normalizing shear stress values to assess orthotropy ratios (dividing by the maximum peak stress value, corresponding to F), we obtained ratios of 1 – 0.47 – 0.31 for Dokos, 1 – 0.65 – 0.53 for Sommer, 1 – 0.27 – 0.47 for Kakaletsis, and 1 – 0.59 – 0.40 for our data. Once again, our results exhibited comparable orthotropy, showing very similar values to the Dokos study, which utilized the same animal model (pig). All studies demonstrate distinct orthotropy, with tissue stiffness being highest in the direction of muscle fibers (F>S>N). Notably, in Kakaletsis' study, stiffness between S and N is inverted, as we have only looked at the positive-shear half of the test and, as mentioned, their study presented significant asymmetries. However, the trend aligns with others in the negative-shear part of their test. Across studies, a reduction of 35-50% in stiffness from the myocytes direction to the intermediate one, and a reduction of 50-70% with respect to the most compliant direction was consistently observed, which is well aligned with our results (41% and 60%, respectively).

4.3. Confined compression experiments

We have analyzed myocardium compressive properties using two types of confined compression tests. In one of them (CC), no fluid was allowed to escape out of the sample, while in the other (FDCC), a small drainage allowed fluid to flow out. CC tests have demonstrated a highly incompressible behavior, reaching volumetric variations up to 10%, but for an average global hydrostatic pressure of about 3.5 MPa (neglecting local differences). These values are much higher than the expected physiological stresses values in any of the tested modes, which are around 10-30 kPa, both in our tests and in the literature [27,28,31,41] (the most extreme case being about 30 kPa recorded by Dokos [27] in the FS-FN configurations of the STS tests). Upon closer inspection, we observe that for the range of hydrostatic pressure relevant to physiological conditions, the volumetric variation is less than 1% (about 0.5% for 30 kPa). Therefore, we can reasonably assume that the myocardium exhibits an incompressible response in the physiological, perfused state, which is consistent with other studies such as [39,42,48]. These results provide direct information on the compressibility of the tissue. To our knowledge, only the study by McEvoy et al. [37] is comparable to ours in the literature. Surprisingly, the results from their study and ours show very pronounced differences. In their case, the maximum recorded pressure values for CC tests are around 50 kPa, similar to those we obtained in the FDCC tests. There are differences in our protocols that difficult the direct comparison between our results: (i) our experiments were performed with fresh tissue in the days following heart extraction, while their hearts were frozen and subsequently thawed; (ii) Our hearts were perfused with cardioplegic solution before extraction, while in their case no perfusion before or after extraction is mentioned; (iii) we imposed the compressive load into the tangential-to-the-epicardium plane, while they exerted the compression on the radial plane (FN and FS planes according to LeGrice coordinates, respectively). Therefore, we propose three potential causes for the recorded differences: (i) differences may be solely due to characterizing fresh versus thawed tissue; (ii) more likely, differences may be attributed to perfusion of the excised heart, as perfused myocardium should behave similarly to end-of-diastole (ED), when myocardium is full of blood, whereas non-perfused tissue will behave similarly to end-of-systole (ES). According to Avazmohammadi et al. [48], ED myocardium can be considered as incompressible ($J = 1$ reported), while ES myocardium is much more compressible ($J = 0.7$ approx. for the medial zone); (iii) differences may be related to the different testing planes, as physiological perfusion occurs epicardium-to-endocardium, making compressibility of the vasculature more influential when compressing on the radial plane than on the tangential plane. This is in line with McEvoy's simulations [37], which state that 40% of the volumetric reduction obtained is due to vascular tissue. We hypothesise that these differences may be attributed to the perfusion state of the tissue, although further research is needed to thoroughly address these questions.

On the other hand, the response observed in the CC tests differs significantly from the FDCC tests, despite maintaining the same protocol. The only distinction is that fluid is allowed to flow out of the sample in the FDCC tests. There, the maximum stress value achieved is reduced by up to two orders of magnitude, down to a value of about 35 kPa. This severe decrease is caused by the fluid drainage, which starts to be expelled already in the volumetric compression stage. Moreover, approximately 200 s after the start of the maintained drainage phase, the recorded pressure reaches its minimum value of about 3 kPa, indicating that the tissue has already completed evacuating all the fluid it could displace and has reached a stable condition. Considering the results of both the CC and FDCC tests, in our perspective, it becomes even clearer that the differences between our tests and McEvoy's are attributed to the drainage of perfused fluid. This implies that in an irrigated state, as may occur in ED, cardiac tissue is highly incompressible, whereas in a drained state (as ES myocardium) still offers compression stiffness, as shown in FDCC, but significantly reduced. These conclusions are in line to what has been reported in the literature [38,39,48], and offer additional insights into tissue compressibility indicating that myocardial behavior is inherently incompressible. However, the 'dynamic' variation in the compressible response throughout the cardiac cycle should not be overlooked.

4.4. Influence of sample location on the mechanical response

True biaxial tests. As mentioned, we also aimed to analyze in depth the local heterogeneities in both radial and longitudinal directions. First, regarding the true biaxial response, we found no significant dependence between the stiffness or anisotropy of specimens and their position along the radial coordinate ($R < 0.169$ in all cases, with $p > 0.517$, Table 4), which is in line with the existing literature [20,28,34]. These results imply a uniform mechanical response from sub-endocardium to sub-epicardium when following orthotropy directions. However, contrary to previous studies [17,22,28], we did observe a slight variation between the AA and the AM zone (Fig. 6a–c). The AA zone exhibited slightly lower stiffness (about 25% and 15% in MFD and CFD, respectively) and lower anisotropy (about 20% less), being the differences in MFD the only ones we have found statistically significant ($p = 0.016$).

Although these differences might be subtle and not all of them have statistical significance, we do believe that they have a physiological justification. We propose that this variation is not because of different tissue behavior between both areas but rather to a greater dispersion of fibers in the AA zone, influenced by ventricular geometry. This results in weaker overall fiber alignment along the MFD and CFD directions. Histological results support this sentence, confirming much lower alignment in AA than in AM (Fig. 5). Despite sampling was standardized and closely monitored in all animals, we observed substantial variations in fiber alignment within the AA region among different animals (not shown herein), with the fiber distribution between animals being much more heterogeneous in the AA zone than in the AM region. In animals with high fiber dispersion in AA, the response was unequivocally isotropic, while in the animals with lower dispersion in the AA zone, the response resembled that of the AM zone.

Therefore, we propose that considering the tissue as homogeneous along the LVFW is appropriate. The observed distinctions between the AM and AA zones are likely attributed to the intrinsic characteristics of the fiber field and the biaxial test itself. Neverthe-

less, we believe that quantifying these differences between the AM and AA zones holds significant value, especially when evaluating tissue properties in a physiological state versus pathological cases such as MI. The location of the infarction and its pre-MI strain-stress state strongly influences the subsequent mechanical properties post-MI [7]. Thus, having a detailed understanding of the physiological local properties can be crucial for quantifying the impact of such pathologies.

Compression tests. We also examined the variations in compressive response along the radial and longitudinal coordinates of the LVFW. To our knowledge, there is no study that has assessed the intrinsic compressibility variation along the LV wall, with the closest being the work proposed by Avazmohammadi, although focused on the 'dynamic' volumetric variations throughout the cardiac cycle along the wall [48].

With respect to the longitudinal coordinate, we have obtained significant differences between the AMFW and AAFW zones in the CC trials ($p = 2.12e\text{-}7$). Although both show highly pronounced incompressible behavior and extremely high hydrostatic pressures, the AAFW zone reached higher-pressure values than the AMFW, indicating greater incompressibility, coinciding with [48]. Despite high deviations in both groups, their behaviors were distinctly differentiated. Conversely, fluid drainage (FDCC) tests demonstrated very similar behavior between both zones, practically coinciding. We did observe some minor differences between the two, such as the peak pressure value reached after volumetric compression and the remaining pressure at the end of the sustained drainage, with no statistical significance ($p > 0.05$).

The same trend was observed along the radial direction in the AMFW area, with significant differences between the SEnd, MIO and SEpi areas in the CC tests ($p < 0.014$). All of them maintained a highly pronounced incompressible behavior, with comparable peak pressure values. In this case, tissue incompressibility increased as we approached the outer part of the wall ($SEpi > MIO > SEnd$), coinciding again with [48]. Considerable deviations were observed in all groups, and the results of MIO partially overlapped with the other two groups. However, general trends were clearly differentiated, and the results of SEpi and SEnd were distant from each other. Once again, FDCC tests demonstrated very similar behavior across all areas ($p > 0.05$).

These findings suggest a certain correlation between the compressive properties of the tissue and its location along the ventricular wall, with significant differences in the CC tests in all analyzed areas, but not in the FDCC tests. As mentioned above, the CC tests are strongly influenced by the presence of perfused fluid in the wall. Although all tested areas exhibited highly incompressible behavior, we hypothesize that variations in incompressibility in CC tests may be related with different vascular volume in each area. Numerous studies have already attempted to characterize volumetric variations along the ventricular wall, primarily focusing on *in vivo* transmural variations [42,48,75–77]. They show an evident transmural gradient, with greater volumetric variation in the subendocardial region and less toward the subepicardial region. This could suggest a higher vascular volume toward the endocardial region, contrary to our results. However, these studies calculate volumetric variations based on 'dynamic' wall deformations, which may not be solely related to a higher vascular volume in each region, but rather to a heterogeneous distribution of deformations within the wall. It is also known that endocardial vessels experience greater emptying during systole due to myocardial wall compression [76,78] (referred to as 'coronary slosh'), which also contributes to more pronounced endocardial variations during the cardiac cycle. Additionally, all these studies rely on implanted beads tracking for volume variation calculations along the myocardial wall. Cheng et al. [77] noted that these heterogeneous variations might be associated with the intervention effects, as they disappeared when measurements were repeated 8 weeks post-implantation.

On the other hand, Feigl et al. reported a higher density of capillaries in the subendocardial region [79], which aligns with the reconstructions presented by Kaimovitz et al. [80,81], showing a greater number of large vessels toward the epicardium and a higher density of small vessels and capillaries toward the endocardium. Based on this, we could hypothesize that the variations in compressibility are more closely related to the differences in vessel sizes in each region, with the epicardium being more incompressible due to a higher number of larger vessels.

Moreover, in the FDCC tests, which are not influenced by the fluid contained in the wall, the response appeared uniform, suggesting that beyond the effects of fluid, the tissue is homogeneous in terms of permeability.

Lastly, both Liu [39] and Avazmohammadi [48] have emphasized the importance of considering a sufficiently large volume (they suggest $>1\ cm^3$) in compressive tests to capture the influence of tissue heterogeneities such as the presence of large vessels. In our study, we selected a considerably smaller representative volume, which might not have captured these punctual events, potentially contributing to the high deviation between samples. We acknowledge this limitation in our study, but we were not able to test larger volumes in compressive experiments.

4.5. Influence of animal age on the mechanical response

4.5.1. Myocardium elastic response

We conducted an analysis of how myocardial elastic response evolve over time by comparing two distinct age groups (4MA and 8MA). Our findings indicate a significant variation in the elastic response of myocardial tissue between these two age groups. Overall, there is a noticeable stiffening of the tissue, with higher strains observed in the 8MA group across all deformation modes ($p < 0.028$ in all cases except FS with $p = 0.12$). A more detailed examination reveals that the increase in stiffness is much more pronounced in CFD-SN-NF-NS (between 91 and 217%) than in MFD-FS-FN-SF (less than 54%), being particularly evident in FS where no statistical significant differences were found between 4MA and 8MA. This distinction is not arbitrary, as in the former group, mechanical stress is primarily absorbed by 'perimysial' collagen fibers, while in the latter, stress is mainly absorbed by myocytes. Indeed, this finding suggests a notable increase in collagen content with the age of the animal, particularly in the 'perimysial' collagen in the N direction. Histological analysis, confirms these results with a significant increase in perimysial collagen content at 8 months of age (Fig. 5). Thus, the remodeling observed during those 4 months has been such as to generate significant changes in the elastic properties of the myocardium. Considering the rapid growth of the pigs, which doubled their original weight in these 4 months, we do believe that such pronounced mechanical and microstructural changes are justifiable. In a related study by Ahmad et al. [32], a comparison of equibiaxial results in 14-day-old and 7-month-old animals also revealed a stiffening of the equibiaxial response with increasing age, albeit their age range differs from our study.

4.5.2. Myocardium compressive response

Regarding myocardial compressive properties, we observed a strong dependence of tissue permeability with increasing age of the animal, but little variability in its incompressibility. The CC tests have demonstrated a very similar response between animals of different ages when compared in the same area. In contrast, the FDCC tests showed very different results for the two ages studied, but little variation depending on the position. This is again due to the differences in tissue microstructure between 4MA and 8MA. As mentioned above, histological analysis revealed evident changes

in the composition of the cardiac tissue, increasing its collagenous component. Since we have analyzed perfused tissue in the CC tests, the similarities between 4MA and 8MA may suggest that the compressible response is still dominated by the fluid, and that there is no substantial change in the tissue's volumetric storage capacity with age. However, a significant reduction in tissue permeability was evident ($p < 6.36e-7$), showing a diminished ability to evacuate fluid, as is visible in all the evaluated variables for the FDCC tests.

To gain further insight into the fluid evacuation capability, we also investigated the temporal variation of the hydrostatic pressure ($\dot{P} = dP/dt$) and the duration from peak compressive load to 90% depressurization (T90). Fig. 7 illustrates the maximum values of each parameter for all the analyzed groups. For 4MA, there was no significant variance radially ($p > 0.06$ in all cases), whereas longitudinally, the AAFW region displayed higher pressure variation ($p = 3.37e-6$) and faster T90 ($p = 0.0014$) compared to AMFW. This indicates a greater fluid evacuation potential in the apical region, possibly due to variances in vasculature between the two regions. Conversely, a notable decrease in $\dot{P}$ is evident in 8MA ($p < 6.57e-10$ in both areas), as well as an important increase in its depressurization time ($p < 6.36e-7$ in both areas), surpassing the variations observed in different areas of 4MA animals. This confirms that older animals tend to reduce its capacity to evacuate the stored fluid, likely attributable to microstructural tissue changes.

In light of these findings, we postulate that cardiac tissue becomes less permeable as the collagen network intensifies. While the tissue's intrinsic behavior appears consistent across different ages, the reduction in permeability may have implications for 'dynamic' volumetric variability throughout the cardiac cycle. Recent studies have shown the importance of considering these 'dynamic' effects [39,48], so we believe that these conclusions may be useful for future research.

4.6. Limitations

There are some limitations in this study that need to be addressed. Firstly, the *in vitro* tests may compromise the physiological behavior of the tissue due to potential damage during the cutting process, especially near the cutting edges. The release of residual stresses in the tissue during machining can further influence the results. All these events may imply that the behavior recorded in subsequent tests could be unrepresentative of *in vivo* behavior. This is well-known, and the applicability of *in vivo* parameters has been questioned in several occasions [82,83]. However, we previously tried to address this issue, and have shown that, although not directly, it is possible to use *in vitro* data for *in vivo* applications [84].

Additionally, certain simplifications were made in this study. In all tests, we have assumed a homogeneous sample geometry and perfectly aligned fiber distribution along testing directions (FSN). However, this assumption is only true at the micrometric scale (250-500 μm), and may not be true at the macroscopic level, where myocardial tissue exhibits dispersion and heterogeneities, which we have disregarded. In studies proposed by Avazmohammadi [33,48], these problems are solved by considering a macroscopic sample (around 1 cm^3) from which the actual geometry and three-dimensional fiber distribution are analyzed, either by sequenced histological analysis [33] or by Diffusion Tensor Imaging [48]. Then, an inverse analysis is performed to estimate the realistic mechanical response. However, the approach used in this paper in which the geometry and fiber field are considered as homogeneous is the one used by most authors in the field [27,28,32].

In Avazmohammadi's 2018 [33], they also highlighted the importance of analyzing the optimality of the testing protocol selected. This approach aims to maximize the predictive capacity and the robustness of the mechanical parameters derived from the experimental tests that are needed for the constitutive models in numerical simulations. They claim that this is of particular importance in the myocardium as it is subjected to several simultaneously coupled deformation modes during the cardiac cycle. In their study they compare the optimality of performing only simple shear tests and conclude that it is better to combine them with pure shear tests. However, they do not analyze the optimality of combining biaxial and simple shear tests. In a previous work, we used our biaxial and shear results for numerical applications, reaching good results at least in terms of passive ventricular haemodynamic response [84].

Due to the heterogeneity of test loading conditions and cardiac tissue structure, finite element modeling would be highly beneficial to validate and corroborate our three-dimensional characterization in a realistic and personalized manner at the microstructural level, but we consider is beyond the scope and objective of our current study, which is focused on the macroscopic response of the myocardium and its heterogeneities considering it as a continuous homogeneous material. Some recent studies, such as [31,37,41] include a microstructural modeling component, but there are also other studies focused solely on the averaged continuous macroscopic aspect, such as [28,32,85]. Nevertheless, due to these heterogeneities both in tissue structure and in loading conditions, finite element analysis may capture the actual tissue response more precisely, so we acknowledge this as a limitation of the study. A more detailed microstructural study combining *in vitro* testing with inverse numerical simulations could be a valuable direction for future work.

Technical challenges were found during the experiments. First, we would like to emphasize the importance of a precise sample preparation to ensure reproducibility. Variability between experiments was observed if samples were collected from different areas in distinct animals or if they were not cut correctly along the FSN directions, leading to the exclusion of some of such samples. Second, the loss of tissue's physiological state was a clear limitation, and tests could not be extended more than 72 h after extraction. We conducted several tests up to 7 days after extraction, but we saw significant differences from 72-96 h (not shown). During the first 72 h we saw no differences as long as the tissue was kept refrigerated and immersed in cardioplegic solution. Consequently, we neither were able to perform all types of tests at every location simultaneously in all animals nor to characterise the compressive response in the F and N directions, only in S. However, other studies also focused the compressive tests only in one direction (F) [37]. However, in all groups considered we obtained a sufficiently large number of samples to perform a well-structured statistical analysis.

Finally, the age study was limited to animals aged 4 and 8 months due to resource and ethical constraints. Although additional age groups would have provided more comprehensive insight, significant differences were observed between the two groups, attributed to rapid growth and increased weight in older animals. Future research could benefit from expanding the age range for a more in depth understanding.

5. Conclusions

We have presented an experimental *in vitro* characterisation methodology to assess the properties of porcine cardiac tissue. We have conducted biaxial and triaxial shear tests to analyze the elastic response of the tissue, as well as confined compression tests for compressibility and fluid flow analysis. Moreover, we explored the mechanical response variations based on sample position and the age of the animal, aiming to improve our understanding of cardiac tissue mechanics.

The elastic response of myocardial tissue exhibited a highly non-linear hyperelastic behavior, anisotropic under biaxial testing and orthotropic under shear testing, which is consistent with existing works in the literature. Position-based analysis showed a homogeneous mechanical response under biaxial tests along both longitudinal and radial coordinates, if microstructural directions (FSN) are considered. Equibiaxial differences between the AAFW and AMFW zones were also quantified. Compared to the AMFW zone, the AAFW exhibited a 25% reduction in maximum stress values and a 20% decrease in tissue anisotropy. Regarding age-related variations, a stiffening of cardiac tissue was observed in all analyzed deformation modes. The increase was notably higher in directions where mechanical stress was absorbed by collagenous fibers (93-217%) compared to those of muscle fibers (46% maximum). Histological studies confirmed a significant increase in collagen content in older animals.

Regarding the compressive response, we observed highly incompressible behavior with a pronounced dependence on fluid content in the myocardial wall. Our results indicate high incompressibility in the perfused state, but significant reductions when fluid exits the myocardial wall, as happens throughout cardiac cycle. We identified highly incompressible and equally permeable behavior across the entire wall, although incompressibility increases towards the outer section of the LV wall and towards the apical zone. In older animals, tissue incompressibility is maintained, but its permeability decreases drastically, diminishing its ability to expel perfused fluid.

To our knowledge, this is the first study to combine a complete three-dimensional elastic characterisation with an analysis of the compressive properties of cardiac tissue as well as a comprehensive investigation onto the variation of local elastic and compressive properties along the LV wall. We hope that our findings will serve for future research aimed at enhancing the understanding of the physiological behavior of cardiac tissue, thereby advancing towards the development of more realistic models and effective therapeutic strategies.

Supplementary data

The complete dataset is accessible to other researchers at: https://doi.org/10.5281/zenodo.12706383

Declaration of competing interest

The authors declare that they have no known competing financial interests or personal relationships that could have appeared to influence the work reported in this paper.

CRediT authorship contribution statement

Nicolás Laita: Writing – original draft, Visualization, Validation, Software, Resources, Methodology, Investigation, Formal analysis, Data curation. **Alejandro Aparici-Gil:** Resources, Methodology, Investigation. **Aida Oliván-Viguera:** Resources, Methodology, Investigation. **Alba Pérez-Martínez:** Resources, Methodology, Investigation. **Miguel Ángel Martínez:** Writing – review & editing, Supervision, Funding acquisition, Formal analysis, Conceptualization. **Manuel Doblaré:** Writing – review & editing, Supervision, Funding acquisition, Formal analysis, Conceptualization. **Estefanía Peña:** Writing – review & editing, Supervision, Funding acquisition, Formal analysis, Conceptualization.

Acknowledgments

This work is supported by the European Union's Horizon 2020 research and innovation programme under grant agreement 874827 (research project BRAV3, C1-BHC-07-2019, H2020); the Next Generations fund of the Spanish Ministry of Science and Innovation through the Cardioprint Project, PLEC2021-008127 and the Spanish Ministry of Economy and Competitiveness through research project PID2022-140219OB-I00. The authors gratefully acknowledge research support from the ICTS "NANBIOSIS", specifically by the Tissue & Scaffold Characterization Unit (U13) of the CIBER in Bioengineering, Biomaterials & Nanomedicne (CIBER-BBN at the University of Zaragoza). CIBER Actions are financed by the Instituto de Salud Carlos III with assistance from the European Regional Development Fund. Authors would also like to gratefully thank our laboratory technician C. Marzo, C. Laita for his help in the figures layout as well as the Central Anatomical Pathology Unit and the Experimental Surgery Service of the Aragon Health Sciences Institute.

References

[1] J.D. Humphrey, Cardiovascular Solid Mechanics: Cells, Tissues, and Organs, Springer Science & Business Media, 2013.
[2] J.W. Holmes, T.K. Borg, J.W. Covell, Structure and mechanics of healing myocardial infarcts, Annu. Rev. Biomed. Eng. 7 (2005) 223–253.
[3] M.R. Zile, C.F. Baicu, W.H. Gaasch, Diastolic heart failure abnormalities in active relaxation and passive stiffness of the left ventricle, N. Engl. J. Med. 350 (19) (2004) 1953–1959.
[4] C. Gutierrez, D.G. Blanchard, Diastolic heart failure: challenges of diagnosis and treatment, Am. Fam. Phys. 69 (11) (2004) 2609–2617.
[5] J.P. Cleutjens, E.E. Creemers, Integration of concepts: cardiac extracellular matrix remodeling after myocardial infarction, J. Card. Fail. 8 (6) (2002) S344–S348.
[6] G.M. Fomovsky, J.W. Holmes, Evolution of scar structure, mechanics, and ventricular function after myocardial infarction in the rat, Am. J. Physiol.-HeartCirc. Physiol. 298 (1) (2010) H221–H228.
[7] G.M. Fomovsky, A.D. Rouillard, J.W. Holmes, Regional mechanics determine collagen fiber structure in healing myocardial infarcts, J. Mol. Cell. Cardiol. 52 (5) (2012) 1083–1090.
[8] M. Castilho, A. van Mil, M. Maher, C.H. Metz, G. Hochleitner, J. Groll, P.A. Doevendans, K. Ito, J.P. Sluijter, J. Malda, Melt electrowriting allows tailored microstructural and mechanical design of scaffolds to advance functional human myocardial tissue formation, Adv. Funct. Mater. 28 (40) (2018) 1803151.
[9] P. Montero-Calle, M. Flandes-Iparraguirre, K. Mountris, A. S de la Nava, N. Laita, R.M. Rosales, O. Iglesias-García, E.M. de Juan-Pardo, F. Atienza, M.E. Fernández-Santos, E. Peña, M. Doblaré, J.J. Gavira, F. Fernández-Avilés, F. Prósper, E. Pueyo, M.M. Mazo, Fabrication of human myocardium using multidimensional modelling of engineered tissues, Biofabrication 14 (4) (2022) 045017.
[10] B. Wang, A. Borazjani, M. Tahai, A.L. de Jongh Curry, D.T. Simionescu, J. Guan, F. To, S.H. Elder, J. Liao, Fabrication of cardiac patch with decellularized porcine myocardial scaffold and bone marrow mononuclear cells, J. Biomed. Mater. Res. Part A 94 (4) (2010) 1100–1110.
[11] A.J. Engler, S. Sen, H.L. Sweeney, D.E. Discher, Matrix elasticity directs stem cell lineage specification, Cell 126 (4) (2006) 677–689.
[12] W. Bian, C.P. Jackman, N. Bursac, Controlling the structural and functional anisotropy of engineered cardiac tissues, Biofabrication 6 (2) (2014) 024109.
[13] J.H. Ahrens, S.G. Uzel, M. Skylar-Scott, M.M. Mata, A. Lu, K.T. Kroll, J.A. Lewis, Programming cellular alignment in engineered cardiac tissue via bioprinting anisotropic organ building blocks, Adv. Mater. 34 (26) (2022) 2200217.
[14] J. Guan, F. Wang, Z. Li, J. Chen, X. Guo, J. Liao, N.I. Moldovan, The stimulation of the cardiac differentiation of mesenchymal stem cells in tissue constructs that mimic myocardium structure and biomechanics, Biomaterials 32 (24) (2011) 5568–5580.
[15] F. Wang, J. Guan, Cellular cardiomyoplasty and cardiac tissue engineering for myocardial therapy, Adv. Drug Deliv. Rev. 62 (7–8) (2010) 784–797.
[16] J.G. Pinto, Y. Fung, Mechanical properties of the heart muscle in the passive state, J. Biomech. 6 (6) (1973) 597–616.
[17] L.L. Demer, F. Yin, Passive biaxial mechanical properties of isolated canine myocardium, J. Physiol. 339 (1) (1983) 615–630.
[18] J. Humphrey, R. Strumpf, F. Yin, Determination of a constitutive relation for passive myocardium: I.- a new functional form and II.- parameter estimation, J. Biomech. Eng. 112 (1990) 333–346.
[19] F.C. Yin, R.K. Strumpf, P.H. Chew, S.L. Zeger, Quantification of the mechanical properties of noncontracting canine myocardium under simultaneous biaxial loading, J. Biomech. 20 (6) (1987) 577–589.
[20] V.P. Novak, F. Yin, J. Humphrey, Regional mechanical properties of passive myocardium, J. Biomech. 27 (4) (1994) 403–412.
[21] M. Sacks, C. Chuong, Biaxial mechanical properties of passive right ventricular free wall myocardium, J. Biomech. Eng. 115 (1993) 202–205.
[22] H. Ghaemi, K. Behdinan, A. Spence, In vitro technique in estimation of passive mechanical properties of bovine heart: Part I. Experimental techniques and data, Med. Eng. Phys. 31 (1) (2009) 76–82.

[23] M.R. Hill, M.A. Simon, D. Valdez-Jasso, W. Zhang, H.C. Champion, M.S. Sacks, Structural and mechanical adaptations of right ventricle free wall myocardium to pressure overload, Ann. Biomed. Eng. 42 (12) (2014) 2451–2465.
[24] I.J. LeGrice, B. Smaill, L. Chai, S. Edgar, J. Gavin, P.J. Hunter, Laminar structure of the heart: ventricular myocyte arrangement and connective tissue architecture in the dog, Am. J. Physiol.-HeartCirc. Physiol. 269 (2) (1995) H571–H582.
[25] G.A. Holzapfel, R.W. Ogden, On planar biaxial tests for anisotropic nonlinearly elastic solids. A continuum mechanical framework, Math. Mech. Solids 14 (5) (2009) 474–489.
[26] H.M. Spotnitz, W.D. Spotnitz, T.S. Cottrell, D. Spiro, E.H. Sonnenblick, Cellular basis for volume related wall thickness changes in the rat left ventricle, J. Mol. Cell. Cardiol. 6 (4) (1974) 317–331.
[27] S. Dokos, B.H. Smaill, A.A. Young, I.J. LeGrice, Shear properties of passive ventricular myocardium, Am. J. Physiol.-HeartCirc. Physiol. 283 (6) (2002) H2650–H2659.
[28] G. Sommer, A.J. Schriefl, M. Andrä, M. Sacherer, C. Viertler, H. Wolinski, G.A. Holzapfel, Biomechanical properties and microstructure of human ventricular myocardium, Acta Biomater. 24 (2015) 172–192.
[29] F. Nemavhola, Study of biaxial mechanical properties of the passive pig heart: material characterisation and categorisation of regional differences, Int. J. Mech. Mater.Eng. 16 (1) (2021) 1–14.
[30] H. Ngwangwa, F. Nemavhola, T. Pandelani, M. Msibi, I. Mabuda, N. Davies, T. Franz, Determination of cross-directional and cross-wall variations of passive biaxial mechanical properties of rat myocardia, Processes 10 (4) (2022) 629.
[31] S. Kakaletsis, W.D. Meador, M. Mathur, G.P. Sugerman, T. Jazwiec, M. Malinowski, E. Lejeune, T.A. Timek, M.K. Rausch, Right ventricular myocardial mechanics: multi-modal deformation, microstructure, modeling, and comparison to the left ventricle, Acta Biomater. 123 (2021) 154–166.
[32] F. Ahmad, S. Soe, J. Albon, R. Errington, P. Theobald, Quantifying the microstructural and biomechanical changes in the porcine ventricles during growth and remodelling, Acta Biomater. 171 (2023) 166–192.
[33] R. Avazmohammadi, D.S. Li, T. Leahy, E. Shih, J.S. Soares, J.H. Gorman, R.C. Gorman, M.S. Sacks, An integrated inverse model-experimental approach to determine soft tissue three-dimensional constitutive parameters: application to post-infarcted myocardium, Biomech. Model. Mechanobiol. 17 (1) (2018) 31–53.
[34] D. Lin, F. Yin, A multiaxial constitutive law for mammalian left ventricular myocardium in steady-sate barium contracture of tetanus, J. Biomech. Eng. 120 (1998) 504–517.
[35] J. Humphrey, R. Strumpf, F. Yin, Biaxial mechanical behavior of excised ventricular epicardium, Am. J. Physiol.-HeartCirc. Physiol. 259 (1) (1990) H101–H108.
[36] T. Kang, J. Humphrey, F. Yin, Comparison of biaxial mechanical properties of excised endocardium and epicardium, Am. J. Physiol.-HeartCirc. Physiol. 270 (6) (1996) H2169–H2176.
[37] E. McEvoy, G.A. Holzapfel, P. McGarry, Compressibility and anisotropy of the ventricular myocardium: experimental analysis and microstructural modeling, J. Biomech. Eng. 140 (8) (2018) 081004.
[38] J.S. Soares, D.S. Li, E. Lai, J.H. Gorman III, R.C. Gorman, M.S. Sacks, Modeling of myocardium compressibility and its impact in computational simulations of the healthy and infarcted heart, in: Functional Imaging and Modelling of the Heart: 9th International Conference, FIMH 2017, Toronto, ON, Canada, June 11-13, 2017, Proceedings 9, Springer, 2017, pp. 493–501.
[39] H. Liu, J.S. Soares, J. Walmsley, D.S. Li, S. Raut, R. Avazmohammadi, P. Iaizzo, M. Palmer, J.H. Gorman III, R.C. Gorman, M.M. Sacks, The impact of myocardial compressibility on organ-level simulations of the normal and infarcted heart, Sci. Rep. 11 (1) (2021) 13466.
[40] P.H. Bovendeerd, W. Kroon, T. Delhaas, Determinants of left ventricular shear strain, Am. J. Physiol.-HeartCirc. Physiol. 297 (3) (2009) H1058–H1068.
[41] D.S. Li, R. Avazmohammadi, S.S. Merchant, T. Kawamura, E.W. Hsu, J.H. Gorman III, R.C. Gorman, M.S. Sacks, Insights into the passive mechanical behavior of left ventricular myocardium using a robust constitutive model based on full 3d kinematics, J. Mech. Behav. Biomed.Mater. 103 (2020) 103508.
[42] H. Ashikaga, B.A. Coppola, K.G. Yamazaki, F.J. Villarreal, J.H. Omens, J.W. Covell, Changes in regional myocardial volume during the cardiac cycle: implications for transmural blood flow and cardiac structure, Am. J. Physiol.-HeartCirc. Physiol. 295 (2) (2008) H610–H618.
[43] L.K. Waldman, Y. Fung, J.W. Covell, Transmural myocardial deformation in the canine left ventricle. normal in vivo three-dimensional finite strains, Circ. Res. 57 (1) (1985) 152–163.
[44] F.J. Villarreal, W. Lew, L.K. Waldman, J.W. Covell, Transmural myocardial deformation in the ischemic canine left ventricle, Circ. Res. 68 (2) (1991) 368–381.
[45] A. Tsamis, W. Bothe, J.-P.E. Kvitting, J.C. Swanson, D.C. Miller, E. Kuhl, Active contraction of cardiac muscle: in vivo characterization of mechanical activation sequences in the beating heart, J. Mech. Behav. Biomed.Materials 4 (7) (2011) 1167–1176.
[46] A. Tsamis, A. Cheng, T.C. Nguyen, F. Langer, D.C. Miller, E. Kuhl, Kinematics of cardiac growth: in vivo characterization of growth tensors and strains, J. Mech. Behav. Biomed.Mater. 8 (2012) 165–177.
[47] X. Zhong, B.S. Spottiswoode, C.H. Meyer, C.M. Kramer, F.H. Epstein, Imaging three-dimensional myocardial mechanics using navigator-gated volumetric spiral cine DENSE MRI, Magn. Resonan. Med. 64 (4) (2010) 1089–1097.
[48] R. Avazmohammadi, J.S. Soares, D.S. Li, T. Eperjesi, J. Pilla, R.C. Gorman, M.S. Sacks, On the in vivo systolic compressibility of left ventricular free wall myocardium in the normal and infarcted heart, J. Biomech. 107 (2020) 109767.
[49] I. Vergroesen, M. Noble, J. Spaan, Intramyocardial blood volume change in first moments of cardiac arrest in anesthetized goats, Am. J. Physiol.-HeartCirc. Physiol. 253 (2) (1987) H307–H316.
[50] F. Yin, C. Chan, R.M. Judd, Compressibility of perfused passive myocardium, Am. J. Physiol.-HeartCirc. Physiol. 271 (5) (1996) H1864–H1870.
[51] A. Oliván-Viguera, M. Pérez-Zabalza, L. García-Mendívil, K.A. Mountris, S. Orós-Rodrigo, E. Ramos-Marquès, J.M. Vallejo-Gil, P.C. Fresneda-Roldán, J. Fañanás-Mastral, M. Vázquez-Sancho, M. Matamala-Adell, F. Sorribas-Berjón, J.A. Bellido-Morales, F.J. Mancebón-Sierra, A.S. Vaca-Núñez, C. Ballester-Cuenca, M.A. Marigil, C. Pastor, L. Ordovás, R. Köhler, E. Diez, E. Pueyo, Minimally invasive system to reliably characterize ventricular electrophysiology from living donors, Sci. Rep. 10 (1) (2020) 1–13.
[52] Q. Ou, R.R. Abouleisa, X.-L. Tang, H.R. Juhardeen, M.H. Meki, J.M. Miller, G. Giridharan, A. El-Baz, R. Bolli, T.M. Mohamed, Slicing and culturing pig hearts under physiological conditions, JoVE (J. Vis. Exp.) 1 (157) (2020) e60913.
[53] S.A. Watson, M. Scigliano, I. Bardi, R. Ascione, C.M. Terracciano, F. Perbellini, Preparation of viable adult ventricular myocardial slices from large and small mammals, Nat. Protoc. 12 (12) (2017) 2623–2639.
[54] G. Plank, R.A. Burton, P. Hales, M. Bishop, T. Mansoori, M.O. Bernabeu, A. Garny, A.J. Prassl, C. Bollensdorff, F. Mason, F. Mahmood, B. Rodriguez, V. Grau, J.E. Schneider, D. Gavaghan, P. Kohl, Generation of histo-anatomically representative models of the individual heart: tools and application, Philos. Trans. R. Soc. A Math. Phys. Eng. Sci. 367 (1896) (2009) 2257–2292.
[55] R.S. Stephenson, A. Atkinson, P. Kottas, F. Perde, F. Jafarzadeh, M. Bateman, P.A. Iaizzo, J. Zhao, H. Zhang, R.H. Anderson, J.C. Jarvis, H. Dobrzynski, High resolution 3-dimensional imaging of the human cardiac conduction system from microanatomy to mathematical modeling, Sci. Rep. 7 (1) (2017) 1–13.
[56] G. Sommer, D.C. Haspinger, M. Andrä, M. Sacherer, C. Viertler, P. Regitnig, G.A. Holzapfel, Quantification of shear deformations and corresponding stresses in the biaxially tested human myocardium, Ann. Biomed. Eng. 43 (10) (2015) 2334–2348.
[57] V. Alastrué, E. Peña, M. Martínez, M. Doblaré, Experimental study and constitutive modelling of the passive mechanical properties of the ovine infrarenal vena cava tissue, J. Biomech. 41 (14) (2008) 3038–3045.
[58] P. Martins, E. Peña, B. Calvo, M. Doblaré, T. Mascarenhas, R. Natal Jorge, A. Ferreira, Prediction of nonlinear elastic behaviour of vaginal tissue: experimental results and model formulation, Comput. Methods Biomech. Biomed.Eng. 13 (3) (2010) 327–337.
[59] A. García, E. Peña, A. Laborda, F. Lostalé, M. De Gregorio, M. Doblaré, M. Martínez, Experimental study and constitutive modelling of the passive mechanical properties of the porcine carotid artery and its relation to histological analysis: implications in animal cardiovascular device trials, Med. Eng. Phys. 33 (6) (2011) 665–676.
[60] J.A. Peña, M.A. Martínez, E. Peña, Layer-specific residual deformations and uniaxial and biaxial mechanical properties of thoracic porcine aorta, J. Mech. Behav. Biomed.Mater. 50 (2015) 55–69.
[61] J.A. Peña, V. Corral, M.A. Martinez, E. Pena, Over length quantification of the multiaxial mechanical properties of the ascending, descending and abdominal aorta using digital image correlation, J. Mech. Behav. Biomed.Mater. 77 (2018) 434–445.
[62] E. Peña, P. Martins, T. Mascarenhas, R.N. Jorge, A. Ferreira, M. Doblaré, B. Calvo, Mechanical characterization of the softening behavior of human vaginal tissue, J. Mech. Behav. Biomed.Mater. 4 (3) (2011) 275–283.
[63] P. Martins, E. Peña, R.N. Jorge, A. Santos, L. Santos, T. Mascarenhas, B. Calvo, Mechanical characterization and constitutive modelling of the damage process in rectus sheath, J. Mech. Behav. Biomed.Mater. 8 (2012) 111–122.
[64] A. García, M.A. Martínez, E. Peña, Determination and modeling of the inelasticity over the length of the porcine carotid artery, J. Biomech. Eng. 135 (3) (2013) 031004.
[65] J. Emery, J. Omens, A. McCulloch, Strain softening in rat left ventricular myocardium, J. Biomech. Eng. 119 (1997) 6–12.
[66] J. Emery, Structural mechanisms of acute ventricular strain softening, Int. J. Cardiovasc. Sci. 1 (1998) 241–250.
[67] D.A. MacKenna, J.H. Omens, A. McCulloch, J.W. Covell, Contribution of collagen matrix to passive left ventricular mechanics in isolated rat hearts, Am. J. Physiol.-HeartCirc. Physiol. 266 (3) (1994) H1007–H1018.
[68] J. Caulfield, T. Borg, The collagen network of the heart, Lab. Invest. J. Tech.Methods Pathol. 40 (3) (1979) 364–372.
[69] H.L. Granzier, T.C. Irving, Passive tension in cardiac muscle: contribution of collagen, titin, microtubules, and intermediate filaments, Biophys. J. 68 (3) (1995) 1027–1044.
[70] K. Wang, R. McCarter, J. Wright, J. Beverly, R. Ramirez-Mitchell, Viscoelasticity of the sarcomere matrix of skeletal muscles. the titin-myosin composite filament is a dual-stage molecular spring, Biophys. J. 64 (4) (1993) 1161–1177.
[71] W.A. Linke, V.I. Popov, G.H. Pollack, Passive and active tension in single cardiac myofibrils, Biophys. J. 67 (2) (1994) 782–792.
[72] W.A. Linke, M.L. Bartoo, M. Ivemeyer, G.H. Pollack, Limits of titin extension in single cardiac myofibrils, J. Muscle Res. Cell Motil. 17 (1996) 425–438.
[73] K.D. Costa, Y. Takayama, A.D. McCulloch, J.W. Covell, Laminar fiber architecture and three-dimensional systolic mechanics in canine ventricular myocardium, Am. J. Physiol.-HeartCirc. Physiol. 276 (2) (1999) H595–H607.
[74] Y. Takayama, K.D. Costa, J.W. Covell, Contribution of laminar myofiber architecture to load-dependent changes in mechanics of LV myocardium, Am. J. Physiol.-HeartCirc. Physiol. 282 (4) (2002) H1510–H1520.
[75] E. Toyota, K. Fujimoto, Y. Ogasawara, T. Kajita, F. Shigeto, T. Matsumoto, M. Goto, F. Kajiya, Dynamic changes in three-dimensional architecture and vas-

cular volume of transmural coronary microvasculature between diastolic-and systolic-arrested rat hearts, Circulation 105 (5) (2002) 621–626.
[76] F. Kajiya, T. Yada, T. Matsumoto, M. Goto, Y. Ogasawara, Intramyocardial influences on blood flow distributions in the myocardial wall, Ann. Biomed. Eng. 28 (2000) 897–902.
[77] A. Cheng, F. Langer, F. Rodriguez, J.C. Criscione, G.T. Daughters, D.C. Miller, N.B. Ingels Jr, Transmural cardiac strains in the lateral wall of the ovine left ventricle, Am. J. Physiol.-HeartCirc. Physiol. 288 (4) (2005) H1546–H1556.
[78] E. Toyota, Y. Ogasawara, O. Hiramatsu, H. Tachibana, F. Kajiya, S. Yamamori, W.M. Chilian, Dynamics of flow velocities in endocardial and epicardial coronary arterioles, Am. J. Physiol.-HeartCirc. Physiol. 288 (4) (2005) H1598–H1603.
[79] E.O. Feigl, Coronary Physiology, volume 63, American Physiological Society, 1983.
[80] B. Kaimovitz, Y. Lanir, G.S. Kassab, Large-scale 3-d geometric reconstruction of the porcine coronary arterial vasculature based on detailed anatomical data, Ann. Biomed. Eng. 33 (2005) 1517–1535.
[81] B. Kaimovitz, Y. Lanir, G.S. Kassab, A full 3-d reconstruction of the entire porcine coronary vasculature, Am. J. Physiol.-HeartCirc. Physiol. 299 (4) (2010) H1064–H1076.
[82] K.D. Costa, J.W. Holmes, A.D. McCulloch, Modelling cardiac mechanical properties in three dimensions, Philos. Trans. R. Soc.London Ser. A Math. Phys. Eng. Sci. 359 (1783) (2001) 1233–1250.
[83] H. Gao, W. Li, L. Cai, C. Berry, X. Luo, Parameter estimation in a Holzapfel–Ogden law for healthy myocardium, J. Eng. Math. 95 (2015) 231–248.
[84] N. Laita, R.M. Rosales, M. Wu, P. Claus, S. Janssens, M.Á. Martínez, M. Doblaré, E. Peña, On modeling the in vivo ventricular passive mechanical behavior from in vitro experimental properties in porcine hearts, Comput. Struct. 292 (2024) 107241.
[85] S. Neelakantan, M. Kumar, E.A. Mendiola, H. Phelan, V. Serpooshan, S. Sadayappan, R. Avazmohammadi, Multiscale characterization of left ventricle active behavior in the mouse, Acta Biomater. 162 (2023) 240–253.